



Tectonic evolution of Macquarie Island: extensional structures and block rotations in oceanic crust[☆]

Ben D. Goscombe^{a,*}, J.L. Everard^b

^aDepartment of Geology and Geophysics, Adelaide University, Adelaide 5005, Australia

^bMineral Resources Tasmania, P.O. Box 56, Rosny Park, Tasmania 7018, Australia

Received 19 March 1998; revised 22 December 1998; accepted 16 August 2000

Abstract

Three distinct tectonic periods are recognized on Macquarie Island. D_1 is a protracted period of palaeo-N–S extension, encompassing initial crust formation at the Proto-Macquarie Spreading Ridge (PMSR), over-printing by late-stage dykes, and a wide range of extensional and dilational structures formed in the near- to off-axis environment. Extensional structures in the lower-crust include fractures, serpentine veinlets, brittle faults, semi-ductile shear zones and ductile mylonites. All were formed in a stress regime with sub-vertical σ_1 and sub-horizontal N-trending σ_3 and are consistent with pure extension in a spreading ridge environment. A minor set of orthogonal fractures and serpentine veinlets suggest a component of along-axis extension during D_1 . Early D_1 tilting of 20–58° around horizontal axes parallel to the ridge axis accompanied growth faults and major differential block uplifts in the near-axis environment. Superimposed on, and in the waning stages of D_1 , was a period of palaeo-NE–SW extension (D_2) with dolerite dyke emplacement. D_2 occurred in a transtensional regime, during transition from extension at the spreading ridge to a transcurrent plate margin (D_3). D_3 constitutes dextral transcurrent movements at the NNE-trending Indo-Australian/Pacific plate margin, active from approximately 10.5 Ma to the present day. Both palaeo-stress analysis of D_3 faults and neotectonic fault scarp geometry indicate dominantly strike-slip and rare thrust events, with NE-trending σ_1 compatible with dextral transpression. Sharp angular discordances in the palaeo-seafloor fabric (D_1 dyke trend), document clockwise rotation of km-scale crustal blocks around vertical axes during D_3 , entirely consistent with dextral transpression at the plate margin. © 2001 Elsevier Science Ltd. All rights reserved.

1. Introduction

Macquarie Island (Fig. 1) is a 150 km² exposure on the Macquarie Ridge that approximately coincides with the plate margin between the Indo-Australian and Pacific oceanic plates. Macquarie Island is comprised entirely of oceanic crust (Varne et al., 1969) and is the only sub-aerial exposure of oceanic crust on Earth that is still within an ocean basin. Because of tilting and differential block uplift, all crustal levels down to and including the mantle lithosphere, are well exposed. Consequently, Macquarie Island offers a unique opportunity to study, by conventional geological mapping techniques, oceanic crust that has not been affected by obduction and is still within its oceanic basin context. Macquarie Island is the only exposure of the Macquarie Ridge, a unique plate boundary type, a trans-

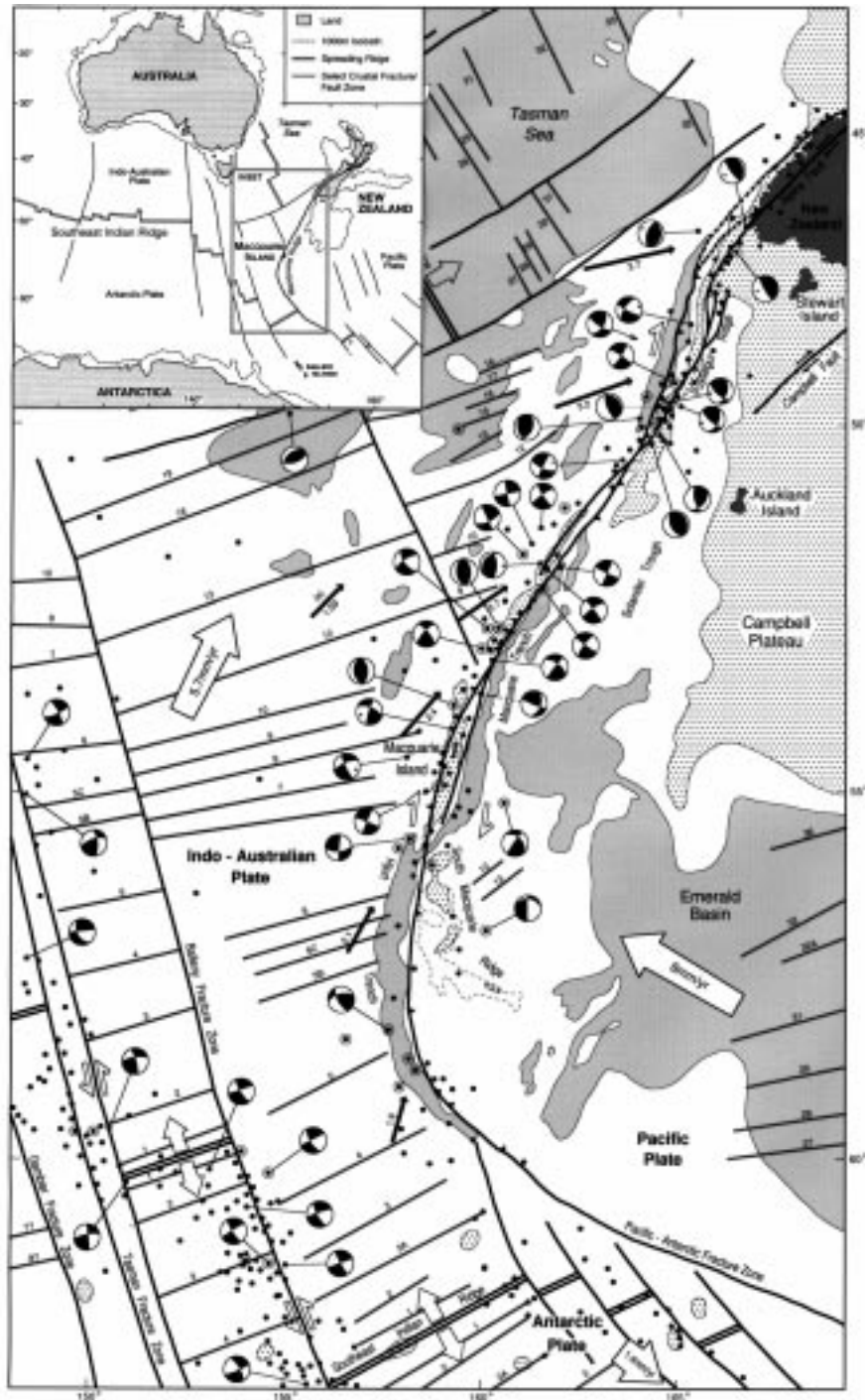
pressional mountain belt at the margin between two oceanic plates. This plate margin is also at a singularly interesting ‘moment’ in its history, in the transition to becoming a subduction zone (Crawford and Coffin, 1993; Collot et al., 1995).









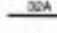

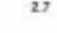


The island was systematically mapped in detail, at 1:5,000 and 1:10,000 scales, for the first time during 1994–1996 (Goscombe and Everard, 1998). Previous workers (Mawson, 1943; Varne et al., 1969; Varne and Rubenach, 1972; Pieters and Wyborn, 1977; Griffin and Varne, 1980; Griffin, 1982; Christodoulou et al., 1984; Duncan and Varne, 1988) mapped the broad distribution of rock types and presented petrological, geochemical and geochronological studies. Few field relationships and no structural analyses were presented. This study presents the first structural analysis of Macquarie Island. We discuss the structural and intrusive history on Macquarie Island and reconstruct the tectonic evolution of this complex region of oceanic crust, focusing on both episodes of block rotation and accompanying faulting and analysis of the wide variety of extensional and dilational structures preserved in the mid- to lower-crust.

[☆] Supplemental material (datafiles in appendices A–E) containing supporting structural and metamorphic data, may be viewed online at <http://veo.elsevier.nl/sg/publish/>

* Corresponding author.

E-mail address: ben.goscombe@adelaide.edu.au (B.D. Goscombe).



-  Land.
-  0 - 2000 metre depth.
-  3000 metre isobath for South Macquarie Ridge only.
-  > 4500 metre depth.
-  Faults and fracture zones.
-  Inferred system of thrust faults indicating approximate boundary between Indo - Australian and Pacific plates, triangles indicate dip direction.
-  Relative movement between crustal plates.
-  Spreading ridge, abandoned ridge indicated.
-  Sea-floor magnetic anomalies.
-  Absolute motion of crustal plates.
-  Direction and rate (cm/yr) of motion of Indo - Australian plate relative to Pacific Plate.
-  Earthquake epicentres: magnitude < 5.5 and > 5.5.
-  Earthquake focal mechanism solution.

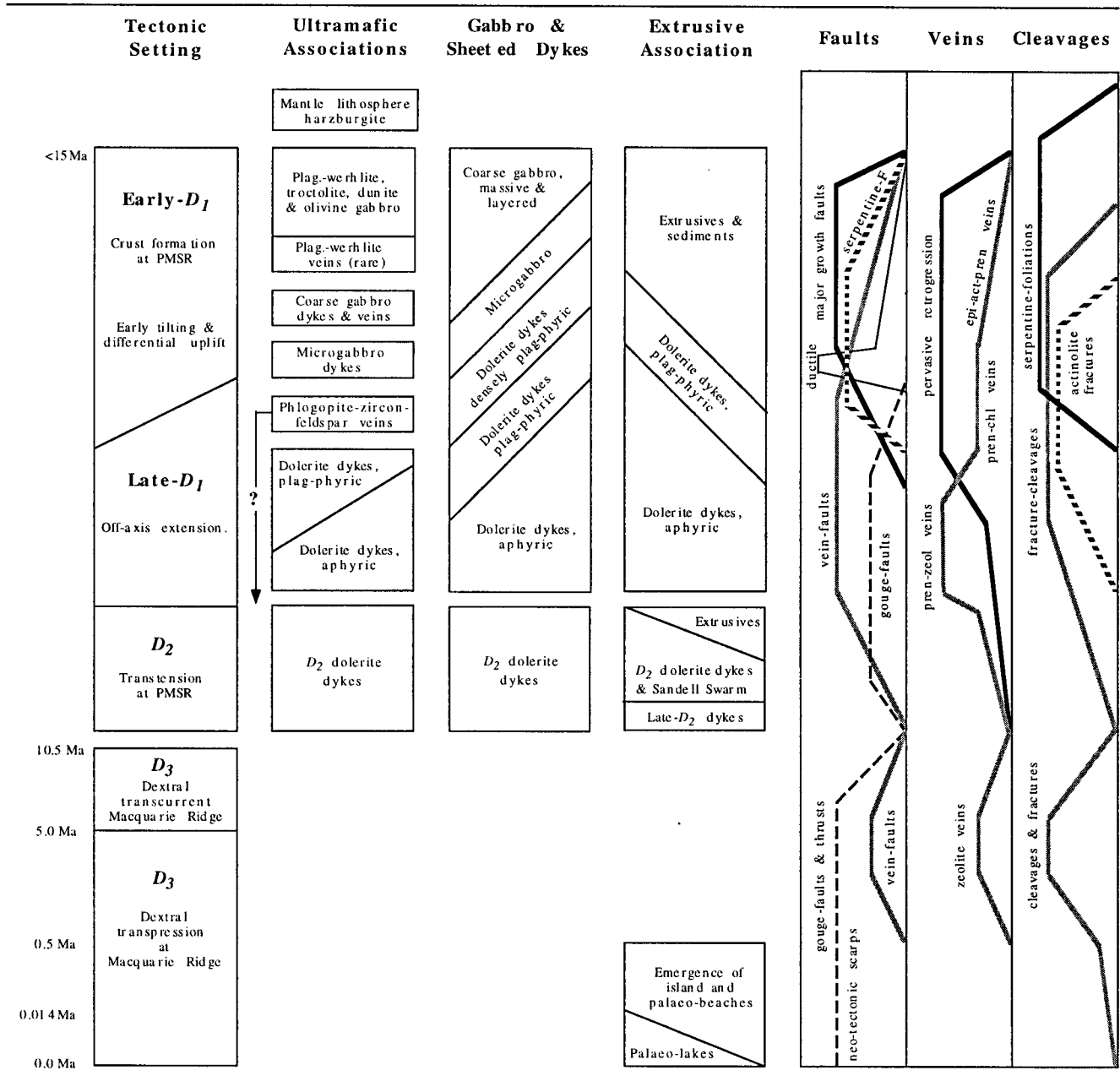


Fig. 2. Summary of igneous and deformational events recognized on Macquarie Island. Time progresses down the page and rock associations of progressively shallower crustal levels towards the right. Proportion/influence of specific structures increases from right to left as indicated by curves. For age correlations see text.

Fig. 1. Tectonic map of Macquarie Ridge region at the present time, with inset of wider Southern Ocean region and major crustal features. Bathymetry after Hayes et al. (1972). The 2000 m depth contour of Campbell Plateau and New Zealand approximately outlines the continental crust; the rest of the map area is oceanic crust. Magnetic anomalies, fracture zones and spreading ridges are after Owen (1983), Veevers (1990) and Sutherland (1995). Absolute plate motions after Larson and Fraymueller (1995). Direction and rate of motion of Indo-Australian plate relative to the Pacific plate after Hayes et al. (1972), Minster and Jordan (1978), Walcott (1978), Coffin et al. (1994) and Collot et al. (1995). Interpretive Indo-Australian/Pacific plate margin and fault motions after Owen (1983), Romanowicz and Ekstrom (1989), Coffin et al. (1994) and Collot et al. (1995). Earthquake epicentres and focal mechanism solutions after Cleary (1966), Sykes (1967), Banghar and Sykes (1969), Johnson and Molnar (1972), Denham (1973), Bock (1981), DeMets et al. (1988), Jones and McCue (1988), Ruff et al. (1989), Romanowicz and Ekstrom (1989), Anderson (1990) and Frohlich et al. (1996).

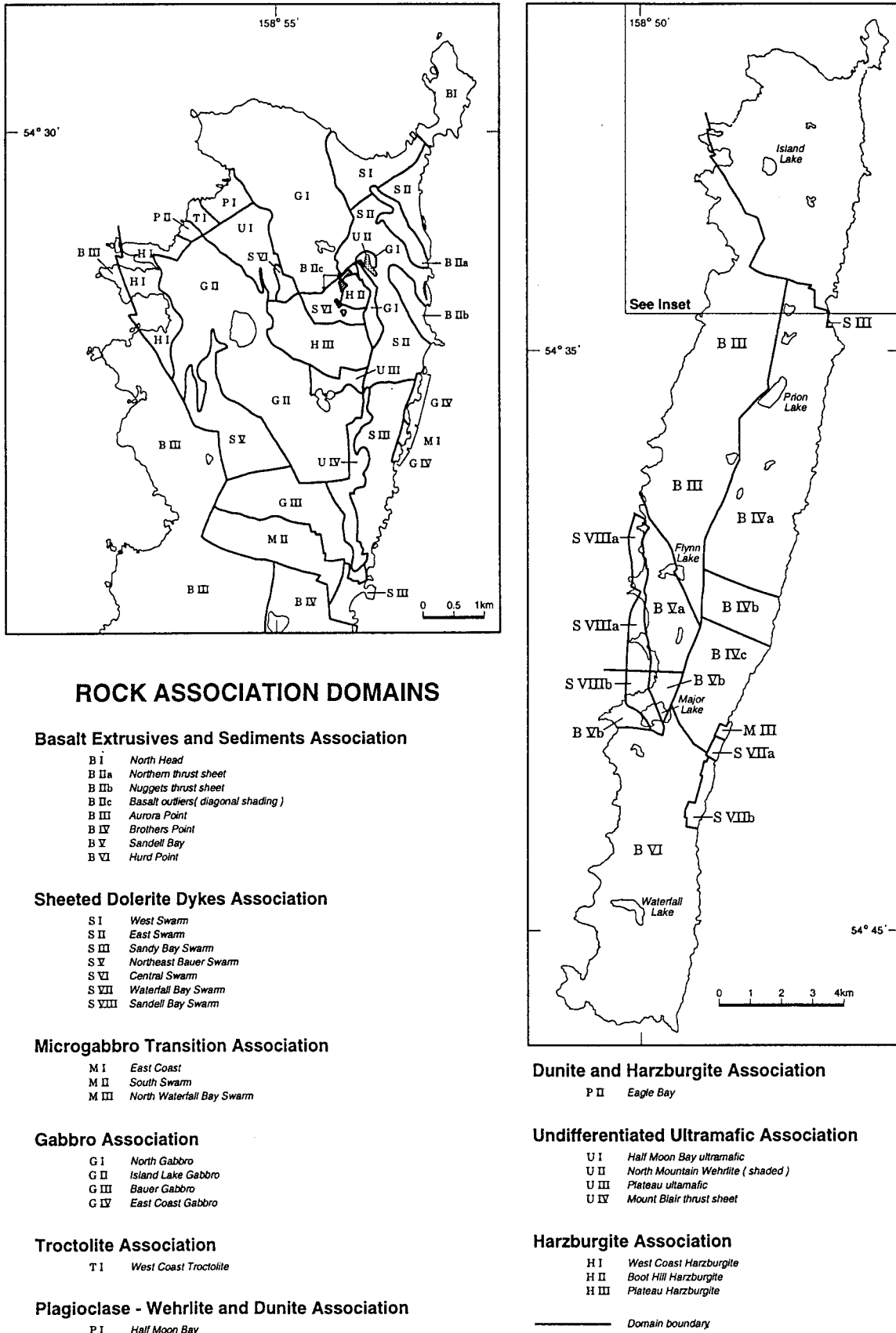


Fig. 3. Map outlining rock association and structural domains referred to throughout this paper. The inset also corresponds to the geological map in Fig. 4.

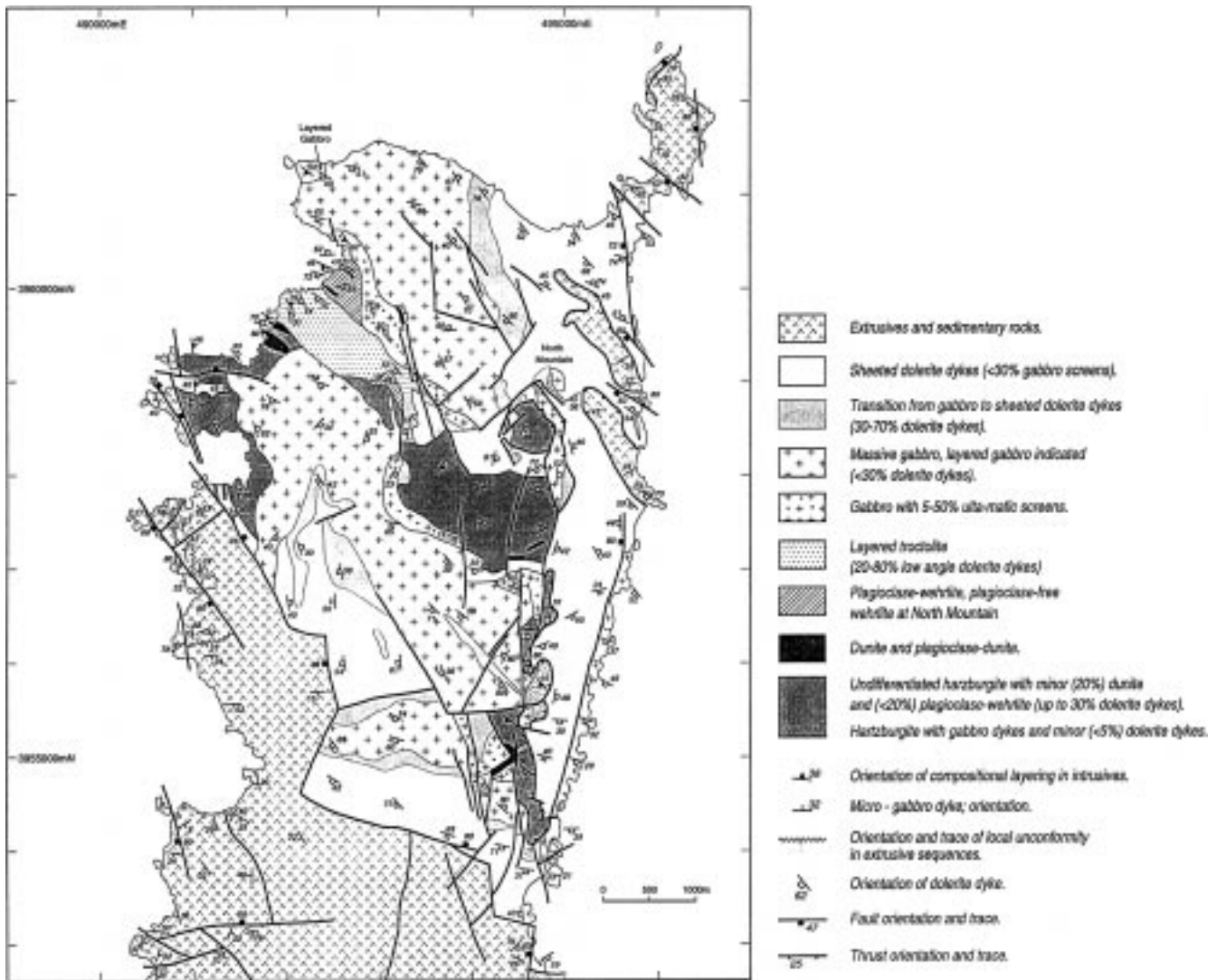


Fig. 4. Simplified geological map of the North Plateau, where essentially all exposures of mid- to lower-crustal rocks occur. Area of map outlined in Fig. 3.

Most studies of structures in lower oceanic crust are either of a remote nature without field relationships, such as studies of drill core and grab samples (Cannat et al., 1992, 1995), or alternatively are from oceanic crust that has been obducted onto continental crust and thus removed from the original tectonic context (Salisbury and Christensen, 1985; Lippard et al., 1986; Nicolas, 1989; Nicolas and Boudier, 1995). The detailed mapping and structural analysis presented here offers a unique opportunity to constrain rock relationships and the temporal and spatial relationships of deformational structures in oceanic crust.

2. Regional geology and tectonic setting

The sector of oceanic crust containing Macquarie Island, between the Tasman Sea oceanic crust and continental crust of the Campbell Plateau, was generated from 39 to 10.5 Ma at the Proto-Macquarie Spreading Ridge (PMSR) that

propagated from the Pacific/Antarctic spreading ridge (Molnar et al., 1975; Weissel et al., 1977; Sutherland, 1995; Lamarche et al., 1997). The PMSR evolved with time from long ridge segments of NNE-trend to short ridge segments of E-trend in the vicinity of Macquarie Island (Lamarche et al., 1997; Schuur et al., 1998). The overall trend of the PMSR was NNE–SSW throughout and roughly coincided with the present day Macquarie Ridge (Lamarche et al., 1997). Plate reconstructions by Molnar et al. (1975), Sutherland (1995) and Lamarche et al. (1997) suggest coincident seafloor spreading and strike–slip movements at the PMSR between 14 and 10.5 Ma.

The present day Indo-Australian/Pacific plate margin is coincident with the Macquarie Ridge, an arcuate 2100 km long crustal fracture system connecting the Pacific/Antarctic and Indo-Australian/Antarctic spreading ridges with the Alpine Fault system in New Zealand (Fig. 1). The Macquarie Ridge evolved from a dextral strike–slip system (10.5–5 Ma) to a transpressional plate margin (5–0 Ma)

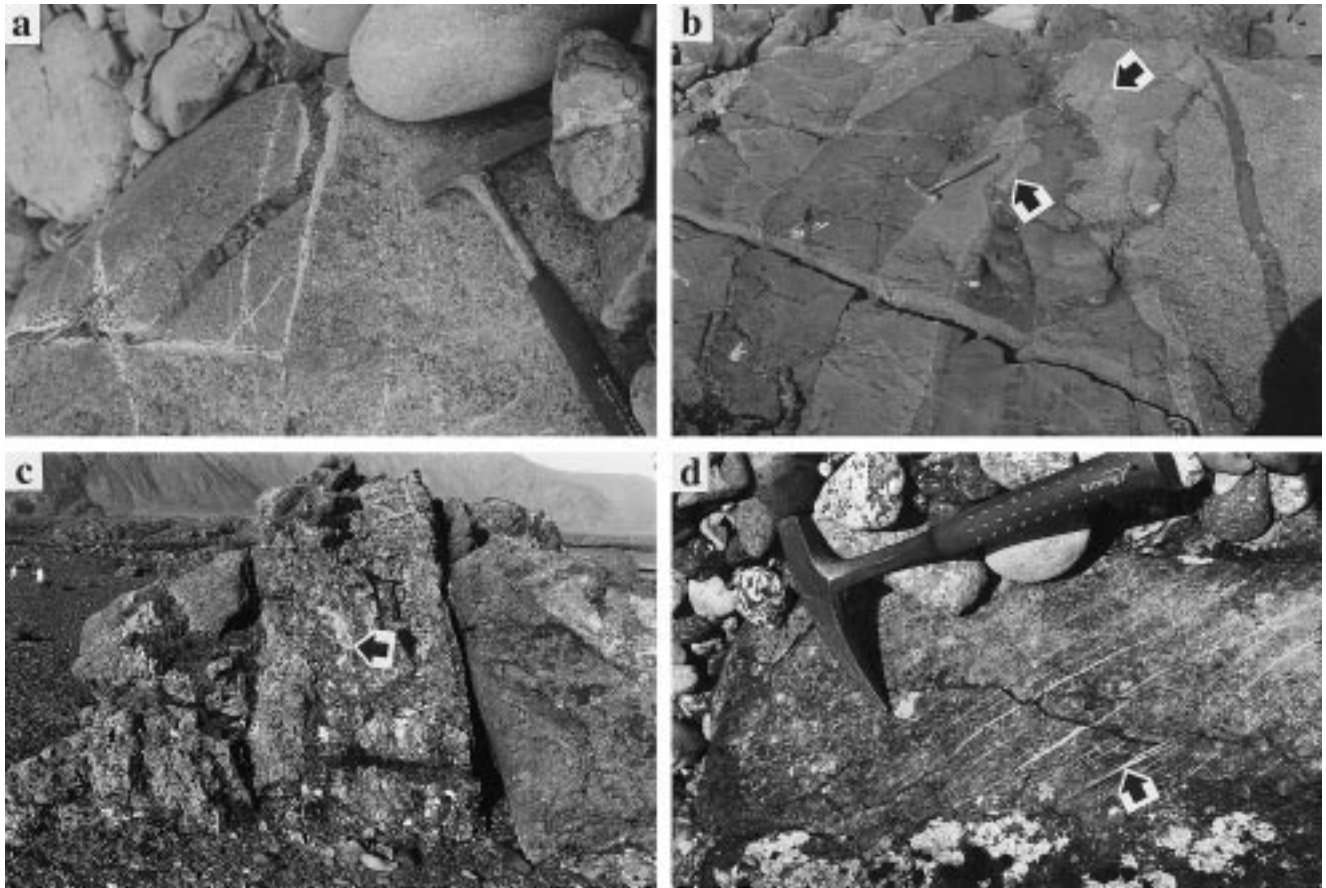


Fig. 5. D_1 dilational structures from middle- and lower-crustal rock associations. (a) Thin dolerite dyke emplaced along pre-existing actinolite-filled fractures with retrogressive halos in gabbro. (b) Packet of sheeted dolerite dykes and enclosed screens of gabbro (indicated). (c) Sub-vertical gabbro dyke in harzburgite, with mylonitized core (indicated). (d) Type-III serpentine-veinlet foliation (indicated) in harzburgite.

(Molnar et al., 1975; Jones and McCue, 1988; DeMets et al., 1988; Frohlich et al., 1996; Schuur et al., 1998). Macquarie Island is in the Central Macquarie Ridge sector, within the plate boundary deformation zone (Fig. 1) and is only 3–5 km east of the steep, 1–5 km wide highly sheared plate margin (Collot et al., 1995; Schuur et al., 1998). In this sector, Bouguer gravity anomalies indicate 150% crustal thickening (Williamson and Johnson, 1974) and focal mechanism solutions are predominantly strike-slip with less common thrust events, indicating a transcurrent plate margin evolving into a subduction zone (Jones and McCue, 1988; Williamson, 1988; Frohlich et al., 1996; Fig. 1).

3. Tectonic framework of events on Macquarie Island

The complex evolution of Macquarie Island crust, from crust formation to the present day, can be assigned to three distinct tectonic periods with different crustal stress fields (Fig. 2). D_1 is a protracted period of palaeo-N–S extension associated with the PMSR, including initial crust formation (Goscombe and Everard, 1997, 1999). Successive intrusive

events (gabbro and dolerite dykes) and a wide variety of extensional deformation structures are superimposed on the newly formed crust, and formed in the near- and off-axis environments. These include ductile and semi-ductile shear zones, dilational foliations, dilational fissures, hydrothermal veins, small-scale vein-filled faults, major growth faults, differential block uplift, block tilting, and formation of scarps and associated talus deposits (Goscombe and Everard, 1999). Over-printing relationships document the evolution of D_1 structures with time (Fig. 2).

D_2 involved palaeo-NE–SW extension and gave rise to rare, late-stage dolerite dykes, hydrothermal veins and possibly also late-stage extrusives. D_2 is interpreted as a transtensional period during transition from D_1 extension to D_3 transcurrent tectonics. D_3 encompasses the entire period of transcurrent and transpressional tectonics, after cessation of extension at the PMSR. D_3 gave rise to major dry gouge-filled faults and associated cleavages, thrust faults, neotectonic fault scarps and vertical-axis block rotations. These structures formed in response to dextral strike-slip and transpression at the Indo-Australian/Pacific plate margin from approximately 10.5 Ma to the present day.

4. Crust formation and rock associations

Macquarie Island was first recognized as oceanic crust by Varne et al. (1969). Detailed geological mapping (Goscombe and Everard, 1998) has identified eight rock associations (Figs. 3 and 4) and has enabled reconstruction of the oceanic crust at the time of formation before dissection by D_1 growth faults and later events (Goscombe and Everard, 1999). The extrusive association is dominated by plagioclase–phyric to aphyric pillow basalts and tabular lava flows (0.5–5%), with minor hyaloclastites, volcanoclastic and talus breccias, hornblende–phyric sills, picrite bodies and rare sediments. Sheeted dolerite dykes display a consistent progression with time from wide, densely plagioclase–phyric dykes to thinner, aphyric dykes. A basal transitional association of microgabbro, contains 20–80% dolerite dykes. Lateral transitions of variable dolerite dyke proportions and coarse gabbro screens, also occur between the coarse gabbro and sheeted dolerite dyke associations [Figs. 4 and 5(b)].

The coarse gabbro association formed as sheeted gabbro mega-dykes (50–300 m wide), with thin parallel screens of pre-existing ultramafic rocks and later minor dolerite and microgabbro dykes (Goscombe and Everard, 1999). The gabbro association is transitional to a well-layered troctolite association with low-angle dolerite sills. The lower-crust consists of two mixed ultramafic associations, both with numerous dolerite dykes and rare coarse-grained gabbro dykes and veins. The uppermost consists of plagioclase–wehrlite with minor troctolite and dunite cumulates. Below this is dominated by dunite, plagioclase–dunite and plagioclase–wehrlite with minor (10–20%) harzburgite and is transitional to the mantle lithosphere harzburgite association. Harzburgite association is only rarely layered and is intruded by numerous coarse-grained gabbro dykes and veins.

5. Gabbro dykes and veins

Coarse-grained gabbro dykes (averaging 270 cm width) and veins (populations averaging 28 cm and 4.5 cm width) are common within and almost exclusive to, the harzburgite association, with few in the other ultramafic associations. Gabbro dykes are concentrated at the margin of harzburgite associations, forming lateral transitions to the coarse gabbro association (Fig. 4) which is contemporaneous with the gabbro dykes in the harzburgites. Dyke margins are straight, unshaped and commonly with microgabbro chill zones. Dykes and veins exploited pre-existing, planar brittle structures such as stepping between serpentine veinlet foliations and fractures. Gabbro intrusions pre-date all dolerite dykes, forming early in D_1 , with 75% post-dating serpentine veinlet foliations suggesting emplacement into relatively cool crust (Fig. 2). Gabbro dykes form a single, well-constrained,

steep orientation set in each domain, with gabbro veins having a similar but wider distribution (Fig. 6; App. A).

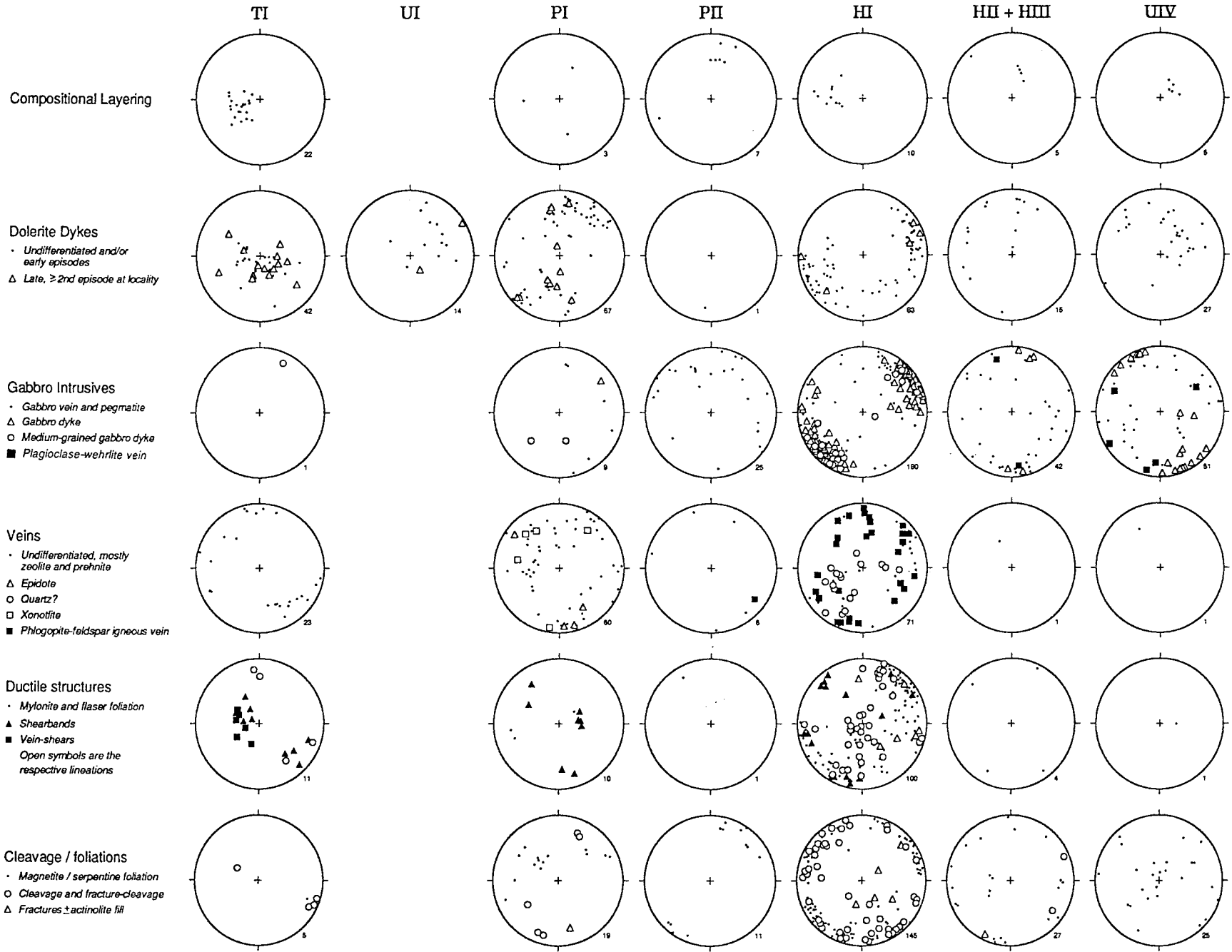
Microgabbro dykes are common in the coarse gabbro association and rare in troctolite and harzburgite associations. They are only 1.5–40 cm wide, with chill zones absent and diffuse margins suggesting emplacement soon after the coarse gabbro host. They post-date coarse gabbro dykes and pre-date all dolerite dykes. Two orientation sets are recognized in domain GI (App. A); sills sub-parallel to compositional layering and vertical dykes.

6. Dolerite dykes

Isolated dolerite dykes constitute the last igneous episode in all rock associations (Fig. 2), with two episodes recognized (D_1 and D_2). Dolerite dykes post-date all ductile deformation and the majority of hydrothermal veins, vein-faults and dilational foliations (Fig. 2). The presence of dolerite dykes in the harzburgite association implies that dolerite dykes constitute a discrete igneous event subsequent to both initial crust formation and differential block uplift of these deep rocks to shallower crustal levels.

Isolated dolerite dykes occur in all rock associations, comprising less than 5–8% of the harzburgite association, 30–50% of other ultramafic associations, 5–15% of the gabbro association and only 1.3–3.3% of the extrusive association. Only in the troctolite association are all dolerite intrusions sub-parallel to compositional layering, being emplaced into coeval sub-ductile extensional shear zones (Fig. 2). The large spread in dyke orientation in the coarse gabbro association (Fig. 7; App. A) is due to intrusion into pre-existing shear zones and fractures (Fig. 5a), and emplacement both as conjugate sets of inclined dykes and as orthogonal sets of sills and sub-vertical dykes. The sheeted dolerite dyke association contains <5% coarse gabbro screens and is dominated by an earliest phase of very thick (>250 cm) densely plagioclase–phyric dykes. Both isolated dykes and late episodes in the sheeted dykes, display a temporal sequence of dyke types varying continuously from thick (100–250 cm), plagioclase–phyric dykes to late-stage, thin (2–10 cm), fine-grained aphyric dykes. A small proportion of dykes in the extrusive association are non-planar with lobate margins that intrude preferentially into inter-pillow spaces, indicating emplacement at very shallow crustal levels.

In most domains, the vast majority of dykes (82–100%; App. B) form a mono-modal distribution around a reasonably well-defined mean orientation (Figs. 6–11; App. A), and these constitute the first (D_1) dyke episode (App. B). D_1 dolerite dykes formed in a near- to off-axis environment in the same stress field as experienced during crust formation. A second episode of dykes (D_2) comprise only 9.3% of all isolated dykes, but locally up to 39–75% of dykes in domains BIVc, BV and BVI (App. B). These consistently strike 45–54° clockwise of the average D_1 dyke strike in



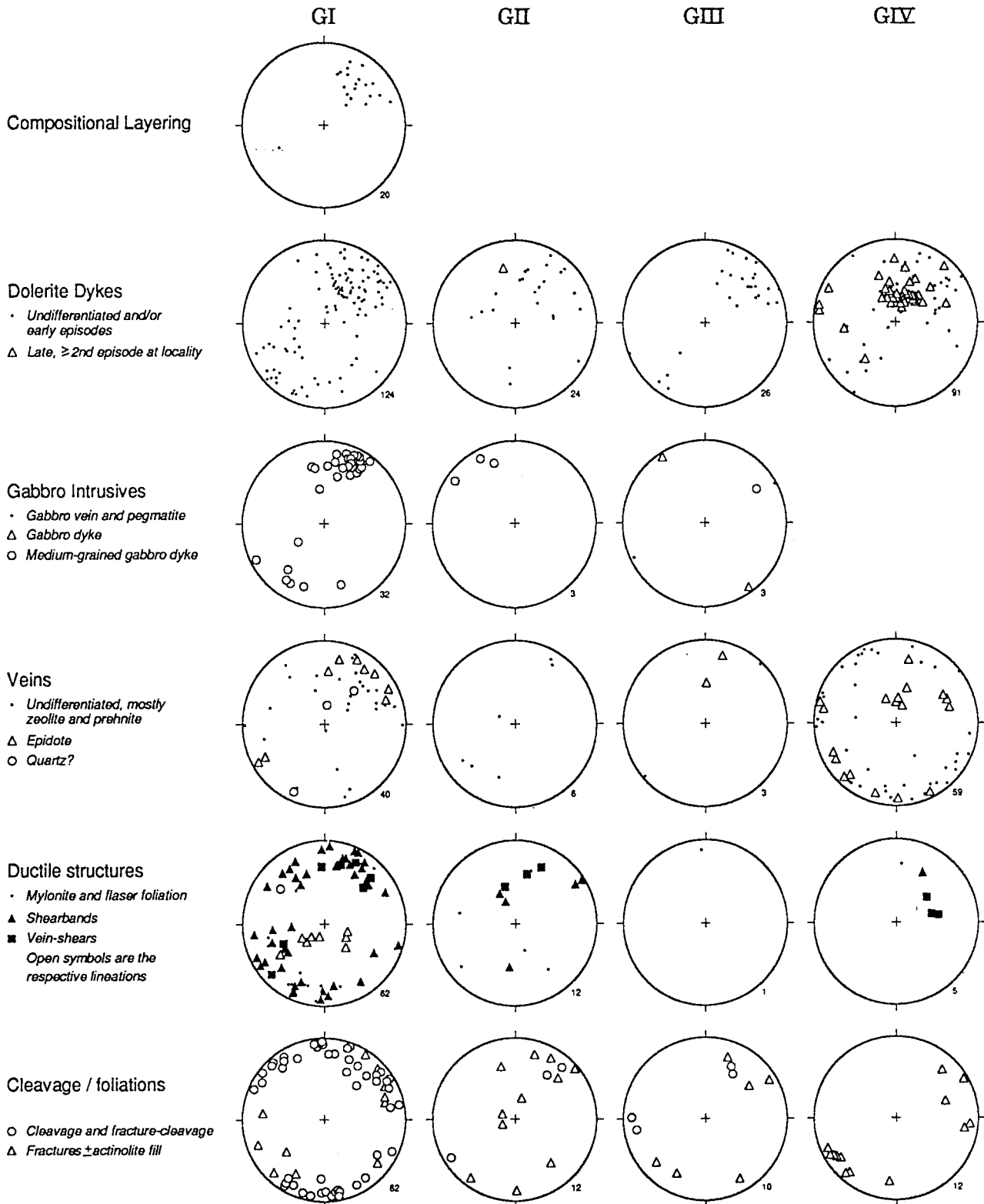


Fig. 7. Lower hemisphere equal area projection of orientation data from the mid-crustal coarse gabbro association domains.

Fig. 6. Lower hemisphere equal area projection of orientation data from the lower-crustal ultramafic rock associations.

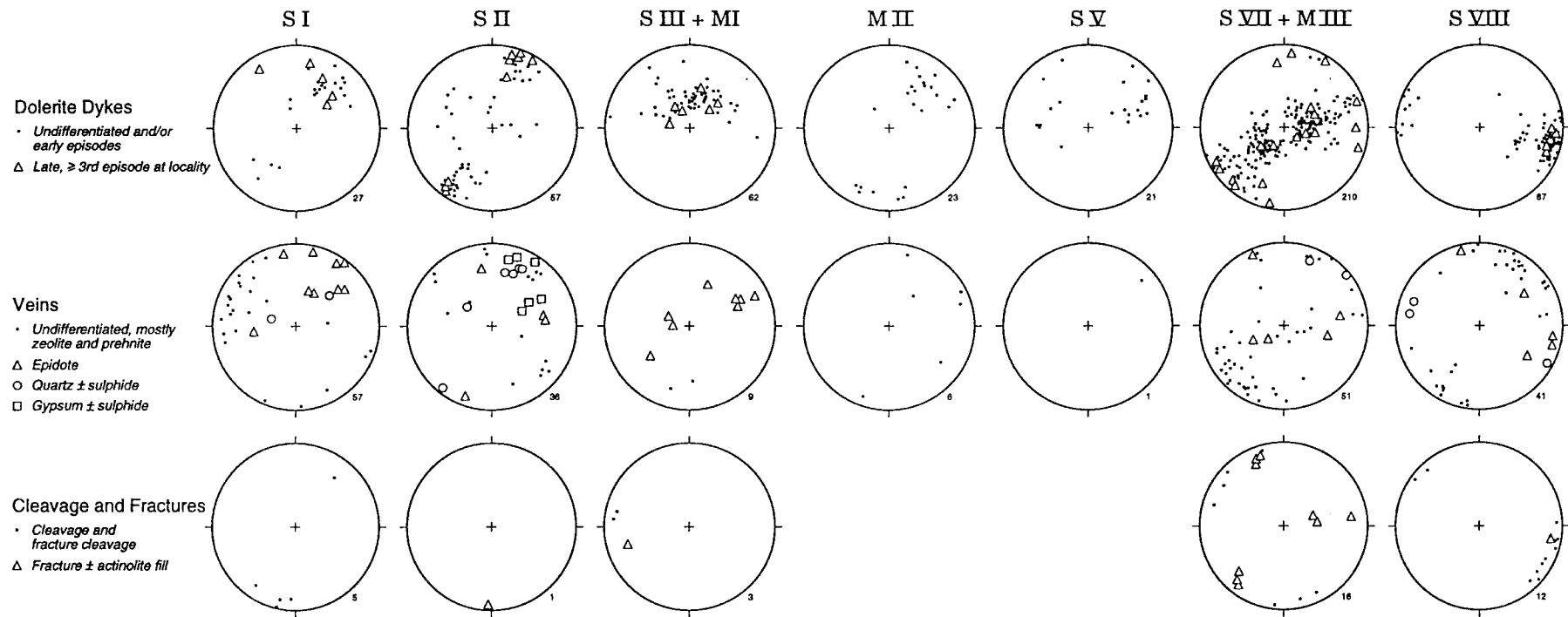


Fig. 8. Lower hemisphere equal area projection of orientation data from the sheeted dolerite dyke and microgabbro transition domains.

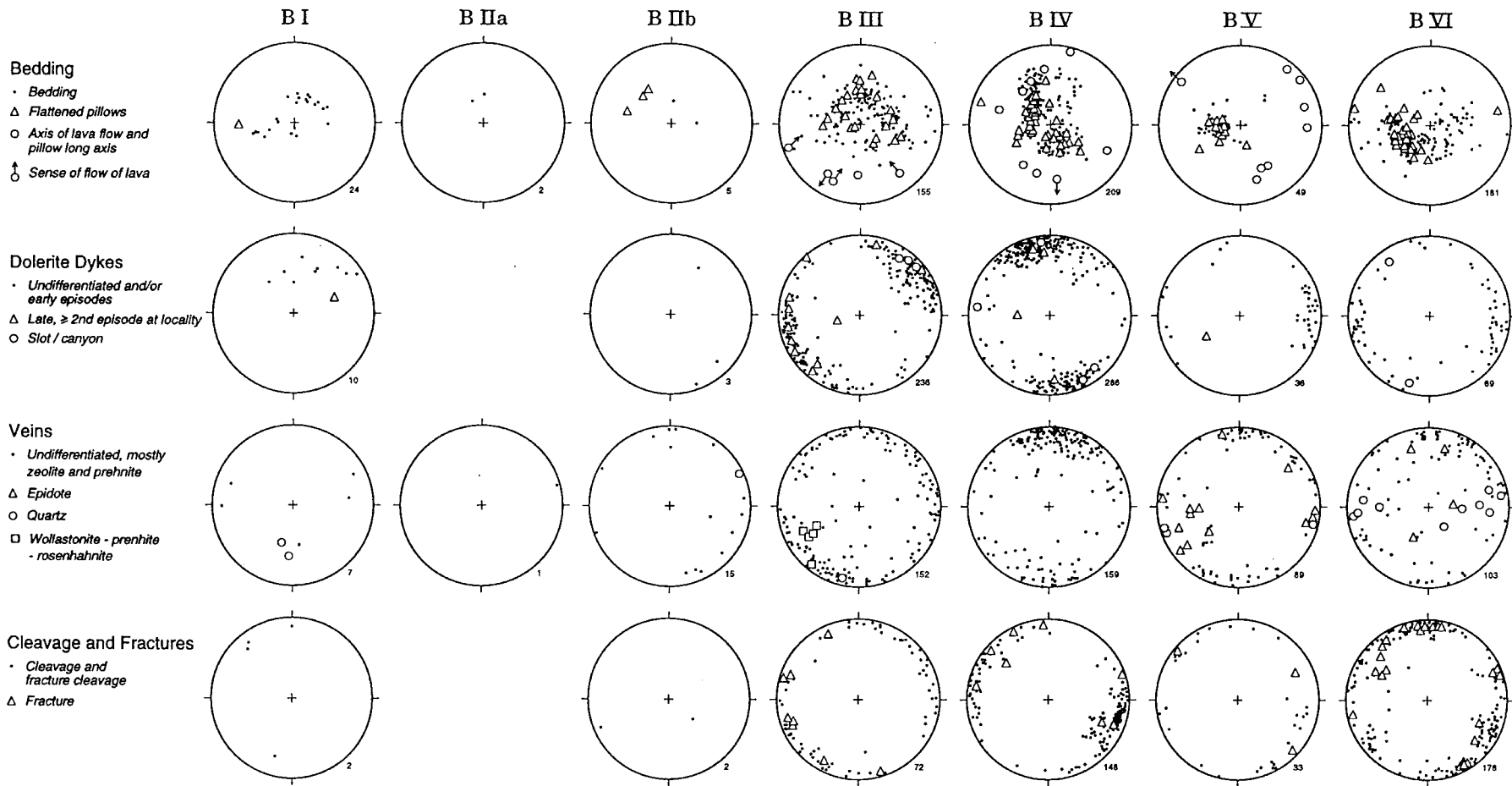


Fig. 9. Lower hemisphere equal area projection of orientation data from the extrusive rock association domains.

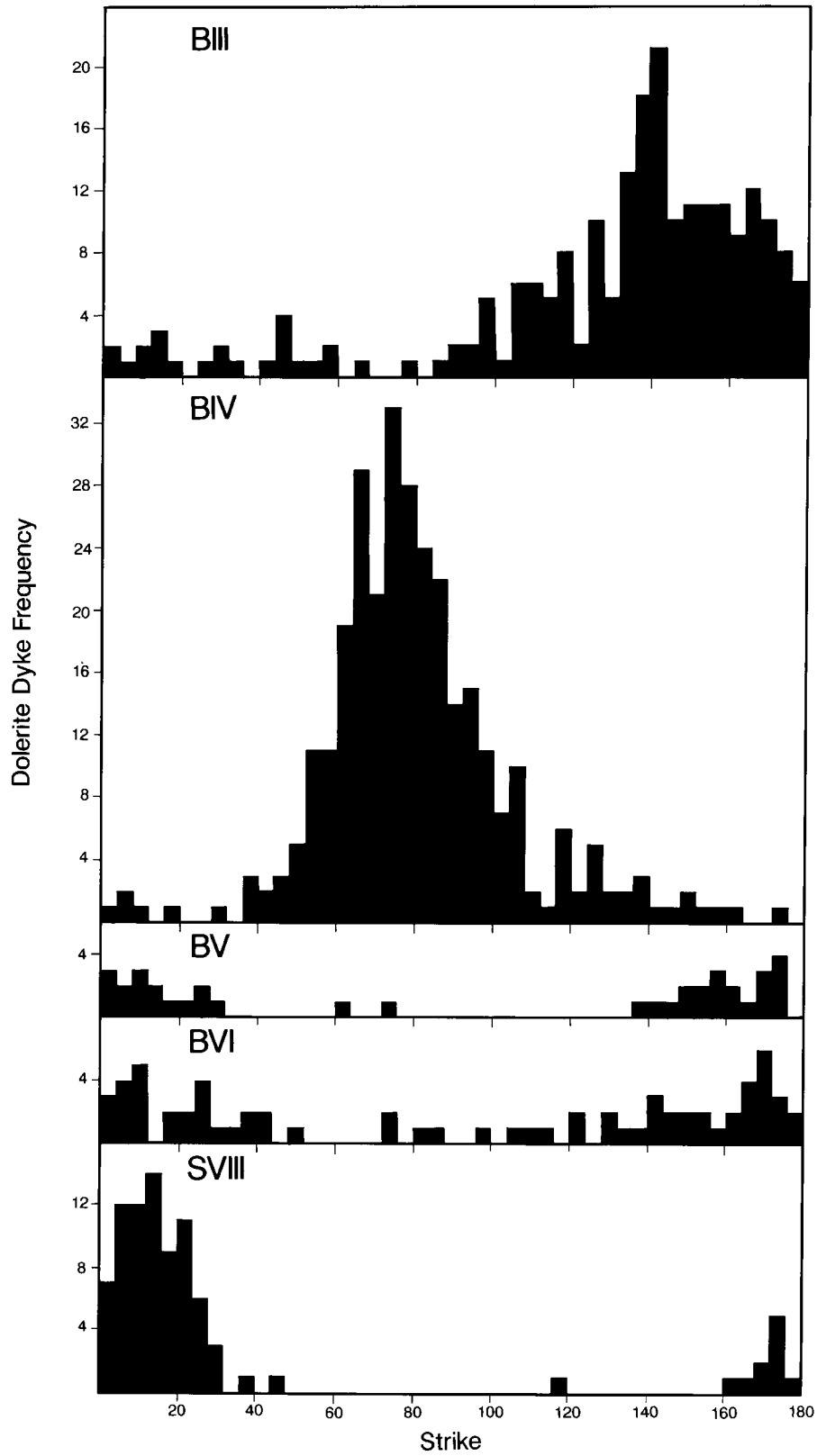


Fig. 10. Frequency distribution of the strike of all D_1 and D_2 isolated dolerite dykes in extrusive association domains and the upper-crustal Sandell Bay Swarm (SVIII).

each domain and almost always (97%) post-date D_1 dykes (Fig. 11b; App. B). D_2 dykes are characterized by being aphyric, sub-vertical, fine-grained, devoid of veins (Fig. 2) and thin, averaging only 29 cm and 81 cm in intrusive and extrusive associations, respectively (App. D). D_2 dykes constitute the only upper-crustal sheeted dyke swarm on the island, the Sandell Bay Swarm (domain SVIII) of 320–500 m width (Figs. 3, 8, 11).

D_1 dykes typically have shallower inclinations than D_2 dykes (App. B), suggesting D_2 dykes post-date all tilting (see below). This infers a real-time break between D_1 and D_2 and suggests D_2 is tectonically unrelated to the spreading ridge environment responsible for tilting of D_1 structures. However, three post- D_2 dykes have orientations consistent with D_1 dykes (App. B), suggesting some temporal overlap between D_1 and D_2 dykes. This suggests a progressive change from D_1 to D_2 extensional stress fields.

7. Dilational fabrics

7.1. Fractures

Fractures are sharp, planar, cracks with very small dilation, distinct from cooling joints by being laterally persistent across lithological contacts. Fractures are typically widely spaced (10–150 cm), with clusters of finely spaced (0.5–15 cm) fractures common in gabbros. Fractures are sub-parallel to the D_1 dyke strike in all domains (Figs. 6 and 7; App. A). Over-printing relations indicate fractures formed predominantly early in D_1 , prior to veins and dolerite dykes (Fig. 5a). Few fractures post-date dolerite dykes and these are parallel to and associated with D_3 faults.

7.2. Actinolite-filled fractures

Planar, laterally persistent, sub-parallel fractures filled with actinolite \pm chlorite \pm hornblende are common in gabbros and often impart a strong foliation. In outcrop, spacing is 2–200 mm and in thin section, fractures form tightly spaced (0.08–1 mm) packets in plagioclase that coalesce into a single fracture in clinopyroxene (Fig. 12a). Fractures bifurcate by stepping along crystallographic cleavage planes, but do not form anastomosing networks. Actinolite-filled fractures are preferentially deflected around pyroxene grains imparting a ‘pseudo-augen’ appearance. Lateral displacements are not apparent, with pure dilation up to 5 mm although typically being only 0.025–1.2 mm. Actinolite-filled fractures post-date ductile fabrics, pre-date both dolerite dykes (Fig. 5a) and hydrothermal veins, and parallel both gabbro and D_1 dolerite dykes (Fig. 7).

7.3. Hydrothermal veins

In gabbros and ultramafic rocks, prehnite (58–78%), epidote (3–30%) and actinolite (\geq 6%) veins dominate,

whereas zeolite veins are absent but become abundant in sheeted dolerite dykes and extrusives. Most veins exhibit pure dilation of 1–120 mm and occur in sets of straight, sub-parallel, laterally continuous veins that are sub-parallel to D_1 dykes (Figs. 6 and 7). Evidence of episodic dilation are rare, and most contain a coarse-grained (0.1–1 mm), homogeneous, unstrained assemblage. Veins are heterogeneously partitioned into 1–100 m wide zones of high spatial density with spacing averaging 11 cm. Almost all veins (95%) post-date D_1 dolerite dykes and pre-date D_2 dykes, with epidote veins invariably being the earliest formed (Fig. 2).

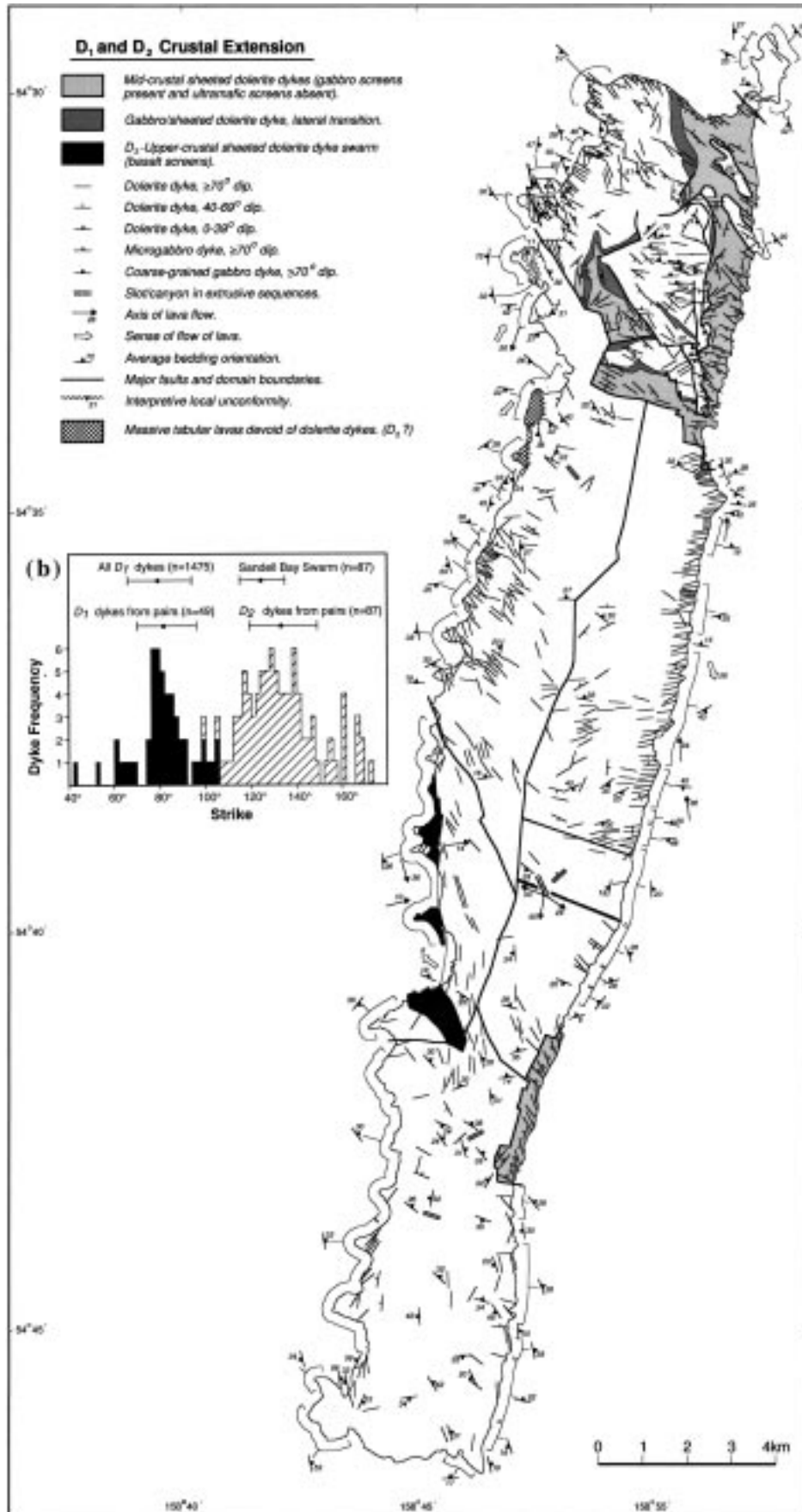
7.4. Fracture-cleavages

Fracture-cleavages common in gabbros and troctolites, constitute a penetrative cleavage comprising planar to curvi-planar, sub-parallel fracture planes with little or no dilation. In contrast to fractures, fracture-cleavages anastomose, are more laterally continuous and very finely spaced (0.06–0.1 mm) within discrete packets of 3–65 mm spacing. Fracture-cleavage planes are deflected around pyroxene grains, crystal clusters and xenoliths, mimicking the appearance of a flattening foliation. However, individual cleavage planes are brittle cracks lacking grain refinement and lateral displacement and formed in an extensional environment. Fracture-cleavages pre-date D_1 dolerite dykes and appear coeval with semi-ductile shear zones and serpentine veinlet foliations (Fig. 2). Most are sub-parallel to D_1 dolerite dykes, with an additional orthogonal set recognized in domains HI and GI (Figs. 6 and 7; App. A).

7.5. Serpentine foliations

Olivine-rich ultramafic rocks develop a consistent temporal sequence of three distinct serpentine \pm magnetite foliation types. Olivine is retrogressed to a mesh texture of serpentine minerals (mostly lizardite) and fine magnetite that predominantly occurs in curvi-planar seams that are median to serpentine bands. Both together define a weak to strong Type-I foliation of 0.05–0.2 mm spacing (Fig. 12b). Serpentine fibres are aligned orthogonal to the magnetite seams, suggesting the rock was under tension with σ_3 aligned normal to the foliation. Type-I foliation is developed only in the olivine matrix and thus envelopes orthopyroxene grains symmetrically, mimicking an apparent ductile foliation. Type-II foliation is defined by rare, straight, widely spaced (0.5–2 mm) magnetite seams that over-print the Type-I foliation at moderate to high angles.

Type-III foliation is defined by thin, laterally extensive, curvi-planar, serpentine veinlets that are sub-parallel to, and invariably post-date, the Type-I foliation (Figs. 5d and 12b). In contrast to Type-I, these are dilational veinlets composed of chrysotile and largely devoid of magnetite. Serpentine fibres are continuous across the veinlet and perpendicular to the vein wall. Veinlets bifurcate but do not anastomose or cross-cut each other, are 0.07–3.00 mm wide and spaced at 4–50 mm. Type-III veinlets split spinel and orthopyroxene



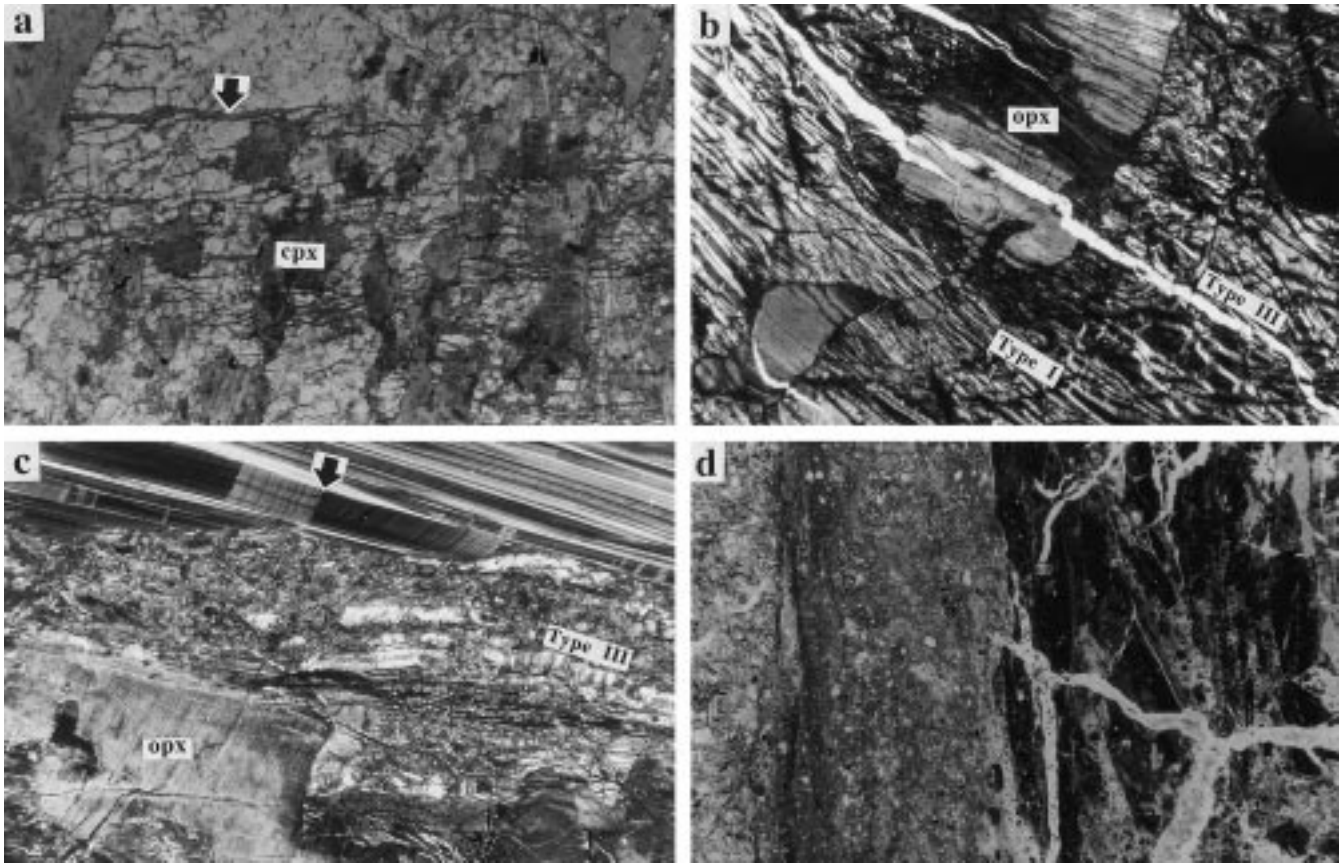


Fig. 12. Microphotographs of dilational foliations and faults from middle- and lower-crustal rock associations. Width of view is 7 mm in all plates. (a) Actinolite-filled fracture-cleavage (indicated) in retrogressed gabbro (plane-polarized light); cpx: clinoproxine. (b) Olivine in harzburgite retrogressed to Type-I foliation of parallel magnetite seams and bands of lizardite with fibres orthogonal to magnetite seams. Type-III serpentinite-veinlet foliation (chrysotile) in centre, dilating orthopyroxene phenocryst, is sub-parallel to Type-I foliation (crossed polars); opx: orthopyroxene. (c) Serpentine-fault with low-angle oblique fibres at the fault margin and multiple episodes of dilation evidenced by domains of discordant growth zoning at high angle to the fibre length (indicated). Note dilational Type-III serpentinite-veinlet foliation parallel to fault in host harzburgite (crossed polars). (d) Vein-fault in dolerite dyke (left). Margin of fault is gouge with increasing prehnite in gouge matrix towards the right. Early gouge in centre of fault (right) is brecciated by syn-tectonic prehnite veining, and also cross-cut by post-tectonic prehnite veins.

phenocrysts by exploiting crystallographic cleavage planes, without lateral displacement (Fig. 12b). Consequently, Type-III foliation formed by dilation of the rock in response to pure extension and constitutes 2–15% extension in individual outcrops. Most Type-III veinlets are sub-parallel to dolerite and gabbro dykes, with a minor orthogonal set evident in most ultramafic domains (Figs. 6 and 7; App. A). Type-III foliation formed throughout a protracted period from prior to gabbro dykes through to the intrusion of D_1 dolerite dykes (Fig. 2).

8. Semi-ductile shearbands

Shearbands are semi-ductile to brittle, straight to curvilinear shear zones with 5–50 cm lateral displacements and

widths of only 0.1–3 cm (Fig. 13b). Margins are sharp to diffuse and typically occur within a wider zone of semi-brittle brecciation. Gabbro and troctolite screens commonly have shearband margins, along which dolerite dykes were preferentially intruded. Shearbands post-date gabbro and microgabbro dykes and pre-date D_1 dolerite dykes (Fig. 2). They are most numerous from the basal gabbro association through to the plagioclase–wehrlite association and may represent a transient brittle–ductile transition in the lower crust as it cooled. Shearbands conform to three orientation sets: steep zones with SE- and NE-strikes and low-angle zones at acute angles (0 – 21°) to compositional layering (Fig. 6; App. A). Mineral aggregate lineations are down dip (Fig. 13b), with normal shear sense, defined by S – C relationships and σ -type porphyroclasts.

Shearband foliation is defined by elongate pressure

Fig. 11. (a) Map of D_1 and D_2 dilational features on Macquarie Island. D_1 and D_2 dykes are not separately represented. Inset (b) of frequency distribution of the palaeo-strike (D_3 effects removed) of D_1 (black) and D_2 (striped) dolerite dykes from pairs with known over-printing relationships (Appendix B).

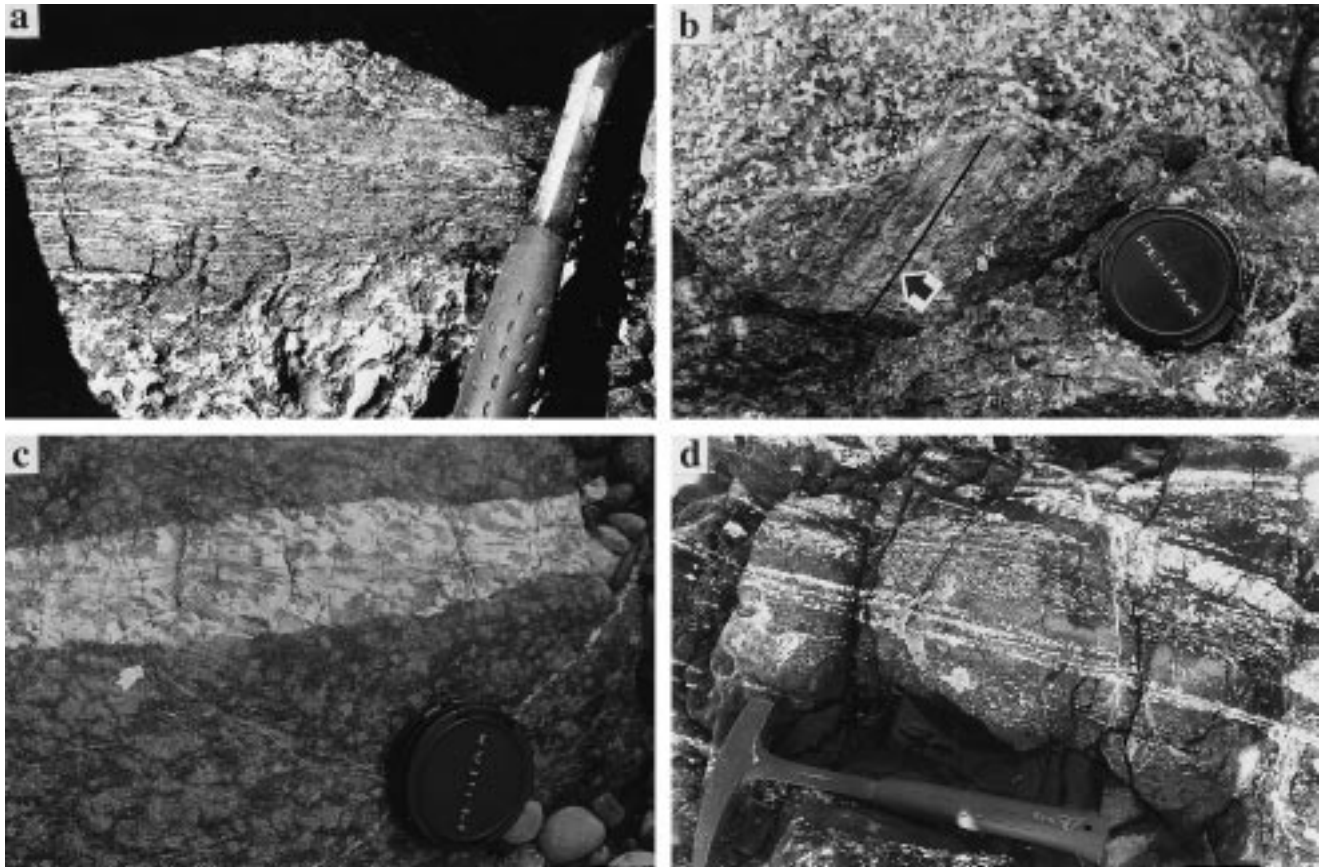


Fig. 13. Ductile and semi-ductile structures in outcrop. (a) Ductile mylonitic shear zone in gabbro dyke. (b) Foliation surface and mineral aggregate lineation (indicated) in semi-ductile shearband in massive gabbro. (c) Gabbro vein in harzburgite, with proto-mylonite core. (d) Magmatic foliation in plagioclase-dunite; plagioclase phenocrysts aligned with compositional layering; no ductile deformation is apparent in thin section.

shadows and mono-mineralic aggregate ribbons of sub-grains (0.1–0.3 mm) derived by semi-ductile to brittle fragmentation of primary plagioclase and clinopyroxene (Fig. 14c and d), and rare aligned actinolite and chlorite. Primary clinopyroxene has undulose extinction, is kinked, boudinaged, stretched into elongate augen (Fig. 14d), and often extremely attenuated into a train of cleavage fragments. Clinopyroxene grain-refinement, though largely brittle, is relatively more ductile than plagioclase grain-refinement. Plagioclase is fragmented and stretched into elongate augen by a random network of micro-faults (Fig. 14c) that are rarely annealed. Thin brittle gouge seams (Fig. 14c) over-print the semi-ductile foliation and comprise 10–90% of the shearband. A proportion of shearbands contain prehnite \pm epidote, either as late-stage but grain-refined veins, or as an integral part of the gouge matrix, implying syntectonic veining.

9. Ductile shear zones

9.1. Ductile deformation in gabbro association and gabbro dykes

All ductile deformation in the ultramafic associations is

partitioned into gabbro dykes and veins. 80% of gabbro dykes contain ductile shear zones and some gabbro veins of only 5 cm width are proto-mylonitized (Fig. 13c). Ductile shear zones are contained wholly within, parallel to and in the core of coarse gabbro intrusions (Figs. 5c and 13c) and pre-date all dolerite dykes. Most ductile shear zones are steep and strike on average 116° (Fig. 7; App. A). Mineral aggregate lineations are mostly down dip with additional shallow plunging sets (Fig. 7). Shear sense defined by σ -type augen and S - C fabrics are predominantly normal and/or dextral. Gabbro dykes were emplaced along brittle dilational structures in an already relatively cool harzburgite, with subsequent ductile deformation being localized within gabbro dykes before they had cooled significantly towards the regional geotherm. Hot gabbro dykes were readily available, though transient, zones that partitioned D_1 extensional strain and when sufficiently cooled, extension was once again partitioned into brittle dilation of the host harzburgite.

Ductile deformation decreases markedly up through the crustal section. Ductile shear zones are absent from gabbro dykes in the plagioclase–wehrlite association (PI) and in the gabbro association occur almost exclusively in the basal-layered gabbros, with few cases at shallower crustal levels. In the gabbro association, ductile deformation is confined to

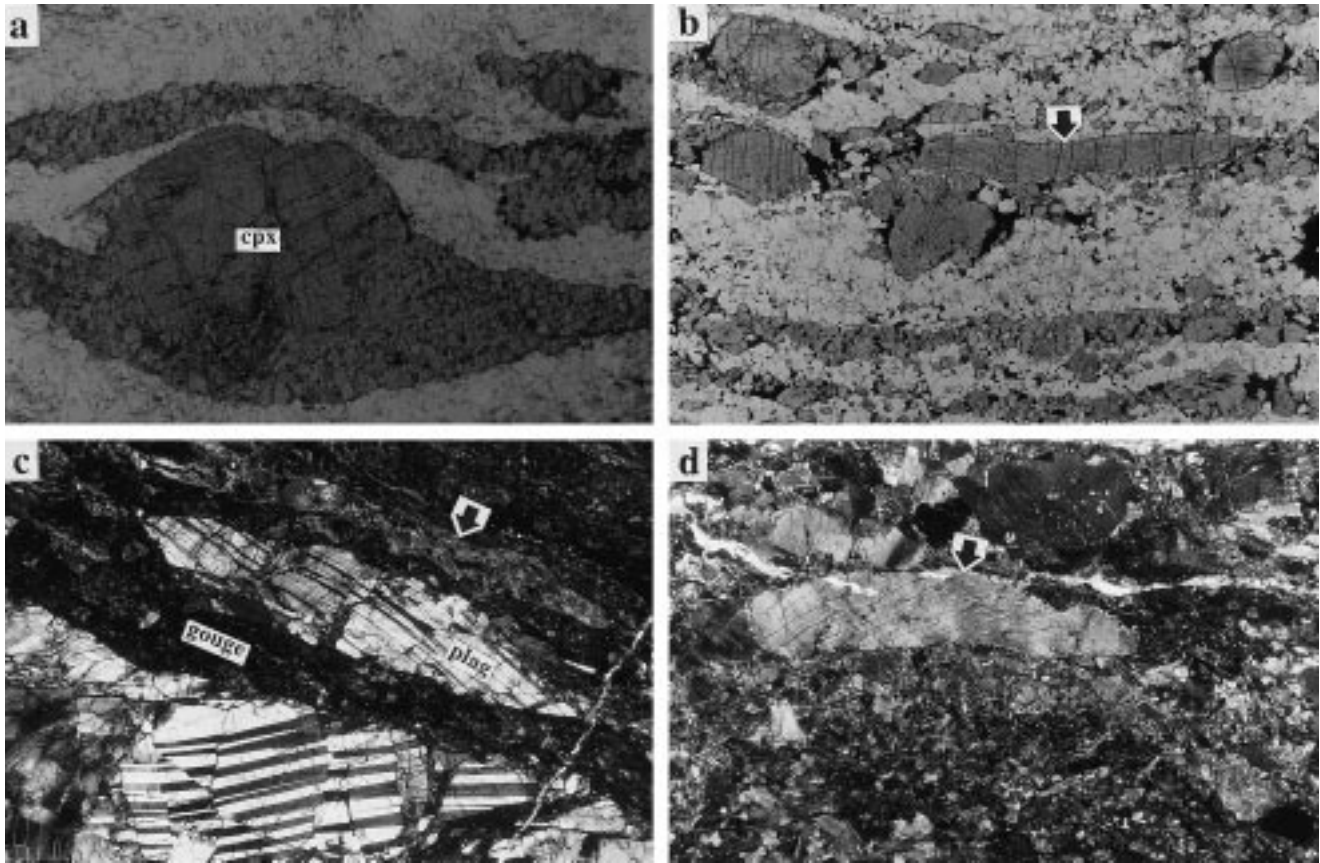


Fig. 14. Microphotographs of semi-ductile and ductile shear zones. Width of view is 7 mm. (a) Primary clinopyroxene asymmetrically mantled by clinopyroxene–orthopyroxene–hornblende aggregate ribbons (plane-polarized light). (b) Ductile stretched orthopyroxene ‘fish’ (indicated) and orthopyroxene–clinopyroxene–ilmenite aggregate ribbons (bottom) (plane-polarized light). (c) Semi-ductile to brittle stretch of plagioclase into elongate augen, by fragmentation and slip along micro-faults. Plagioclase enclosed by brittle gouge zones and trains of clinopyroxene fragments (indicated) (crossed polars). (d) Semi-ductile stretch of clinopyroxene by slip along cleavage planes (indicated) and crenulation. Brittle gouge and clinopyroxene fragments comprise the lower portion of the view (crossed polars).

1–7 cm wide mylonite zones and 0.15–1 cm wide ultra-mylonites, mostly striking 095–119° with moderate northerly dips and normal displacements. In all ductile shear zones there is a consistent temporal sequence partitioning strain into progressively thinner, nested zones with higher degrees of grain refinement and grainsize reduction. This sequence progresses from wide proto-mylonite zones, to a central mylonite (Fig. 13a) averaging 13.5 cm width and 72% grain refinement, and lastly sharply bounded ultra-mylonites of only 1–3 cm width.

The mylonitic foliation (Fig. 13a) is defined by laterally extensive, 0.2–0.7 mm wide, aggregate ribbons of either plagioclase, clinopyroxene–orthopyroxene ± ilmenite ± red phlogopite (Fig. 14a and b), olivine–orthopyroxene–fawn phlogopite or red-brown hornblende–ilmenite–orange phlogopite. Aggregate ribbons, mantles and pressure shadows are derived by ductile recrystallization of primary phases (Fig. 14a), resulting in significant grainsize reduction from mm–cm-scale to 0.03–0.57 mm in mylonites and 0.06–0.17 mm in ultra-mylonites. Aggregate ribbons have annealed granoblastic textures comprising unstrained, equi-

dimensional sub-grains with straight to curvi-planar grain margins (Fig. 14b). Primary phases and orthopyroxene in particular, are stretched to highly elongate augen by slip along crystallographic cleavage planes (Fig. 14b; App. C). Ultra-mylonites experienced >90% grain refinement, leaving rare, very small (<3 mm) porphyroclasts in a polygonal granoblastic matrix containing mono-mineralic aggregate ribbons of plagioclase, green or red-brown hornblende and clinopyroxene.

9.2. Shear strain and flow regime

The strain ellipse is estimated by the aspect ratios of stretched augen, measured in sections cut orthogonal to the principal strain axes (App. C). Normalized aspect ratios, and an average k ratio (Flinn, 1962) of 1.8, indicate strain intermediate between uniaxial extension and plane strain. Because of ductile recrystallization in the matrix, X/Z ratios offer only minimum estimates of bulk strain. Orthopyroxene is the most stretched with X/Z ratios up to 10.8 and averaging 5.6, with averages of 4.1, 4.0 and 3.2 in olivine,

feldspar and clinopyroxene, respectively. *S*–*C* fabrics with acute angles between *C*- and *S*-planes averaging 19°, indicate a shear strain of 2.9 (Ramsay and Graham, 1970). More commonly, co-planar *S*–*C* fabrics are developed, indicating high shear strains (≥ 2.3) (Burg and Laurent, 1978; Berthé et al., 1979). High shear strains are further supported by the high degree of grain-refinement and grain-size reduction in the matrix. *S*–*C* fabrics, σ -type augen (Fig. 14a), pyroxene–‘fish’ (Fig. 14b) and asymmetric curvature of the mylonite foliation into parallelism within the shear zone core (Fig. 13c), all suggest non-coaxial shear (Ramsay, 1979; Berthé et al., 1979; Lister and Snoke, 1984; Passchier and Simpson, 1986). The trans-tensional nature of ductile shear zones is evidenced by the predominance of normal shear-sense and close temporal association with dilational structures, such as emplacement of the gabbro dykes and serpentine veinlet foliation.

9.3. Apparent ‘ductile’ fabrics in ultramafics

There is no evidence of pervasive, regionally extensive ductile deformation in harzburgite and other ultramafic rocks. Orthopyroxene and spinel grains in harzburgite have not experienced ductile recrystallization and remain equant, unaligned and unstrained. Fresh olivine preserves a coarse-grained adcumulate texture with no sub-grain development or grain-shape fabric. This is in contrast to *L*–*S* mantle flow fabrics preserved in harzburgites in the Oman and Bay of Island ophiolites and the Mid-Atlantic Ridge (Girardeau and Nicolas, 1981; Salisbury and Christensen, 1985; Nicolas, 1989; Cannat et al., 1992; Nicolas and Boudier, 1995). All pervasive foliations recognized in Macquarie Island harzburgite are the result of brittle dilation, such as Type-III serpentine veinlets. A ductile grain-shape foliation defined by olivine sub-grains is sub-parallel to compositional layering in only one harzburgite locality and possibly represents early, layer-parallel mantle flow (Nicolas, 1989).

Plagioclase grains, with augen shapes and alignment parallel to compositional layering, are recognized in a few plagioclase–wehrlite and plagioclase–dunite localities (Fig. 13d). No ductile deformation is evident in thin section; plagioclase grain-shape and alignment possibly result from viscous deformation of the magma and crystal alignment parallel to compositional layering (Nicolas, 1989).

10. Brittle faulting

10.1. Fracture-faults

Fracture-faults are reactivated joints and fractures with slickenlines and slickenfibres on the surfaces indicating the movement direction. Fracture-faults appear to be randomly orientated, not laterally persistent and have very small displacements averaging only 2.0 cm. Slickenlines have steep plunges and invariably normal shear-sense,

defined by steps, asymmetrical hollows and vein fibre growth direction. Fracture-faults are coeval with veining and pervasive hydrothermal retrogression during D_1 .

10.2. Serpentine-faults

Pale green, clino-chrysotile-filled faults are developed only in ultramafic rocks and have widths ranging from 0.15–12 cm, with displacements of 1–250 cm. They are curvi-planar with sharp walls and serpentine fibres obliquely continuous from wall to wall (Fig. 12c). Multiple movement events are recognized both as discrete cross-cutting slip-planes and growth zoning domains with different fibre orientation (Fig. 12c). Symmetrical growth zoning indicates that serpentine fibres grew continuously throughout faulting and thus the fibres indicate the true vector of movement between the walls of the faults. Oblique fibre orientations and matching of fault walls indicate that dilation accompanied lateral movements in all serpentine-faults, with no grain refinement of the host recognized. Serpentine-faults are heterogeneously distributed, with most developed in 1–10 m wide zones of intense faulting. Serpentine-faults appear randomly orientated, but all formed in an extensional stress field as indicated by their dilational nature and invariably normal shear-sense. All formed during D_1 , with most post-dating gabbro dykes and pre-dating dolerite dykes (Fig. 2).

10.3. Vein-faults

Vein-faults are gouge and breccia zones containing significant proportions of hydrothermal vein material. They are the most widespread and pervasive type of faulting on the island, with spatial densities as high as 650 faults/km² in the extrusives and are absent only from the harzburgite association. Widths range from 0.1 to 35 cm (averaging 3.9 cm) and displacements from 0.5 to 40 cm. These dimensions are significantly less than dry gouge/breccia faults (see below) and few classify as major faults. They are not very laterally continuous, typically forming anastomosing networks of curvi-planar zones. Slickenlines have moderate plunges in all orientations with shear sense being predominantly (>60%) normal. Multiple slickenline sets in individual faults are common and the latest formed is invariably sub-horizontal, suggesting strike–slip reactivation during D_3 transpression.

Three classes of fault histories are recognized. (1) Most initially formed as foliated gouge zones with later dilation and prehnite \pm epidote or actinolite \pm chlorite veining (Fig. 12d), followed by grain refinement of the vein material. Less common are (2) vein-filled breccia zones and (3) zones of synchronous gouge formation and veining, with veining persisting after the last lateral movement. In all, vein/gouge ratio is high (typically 60–80% vein material), indicating significant dilation accompanying lateral movements, suggesting formation during D_1 . This is supported by over-printing relationships; 70% pre-date both hydrothermal veins and dolerite dykes and 86%

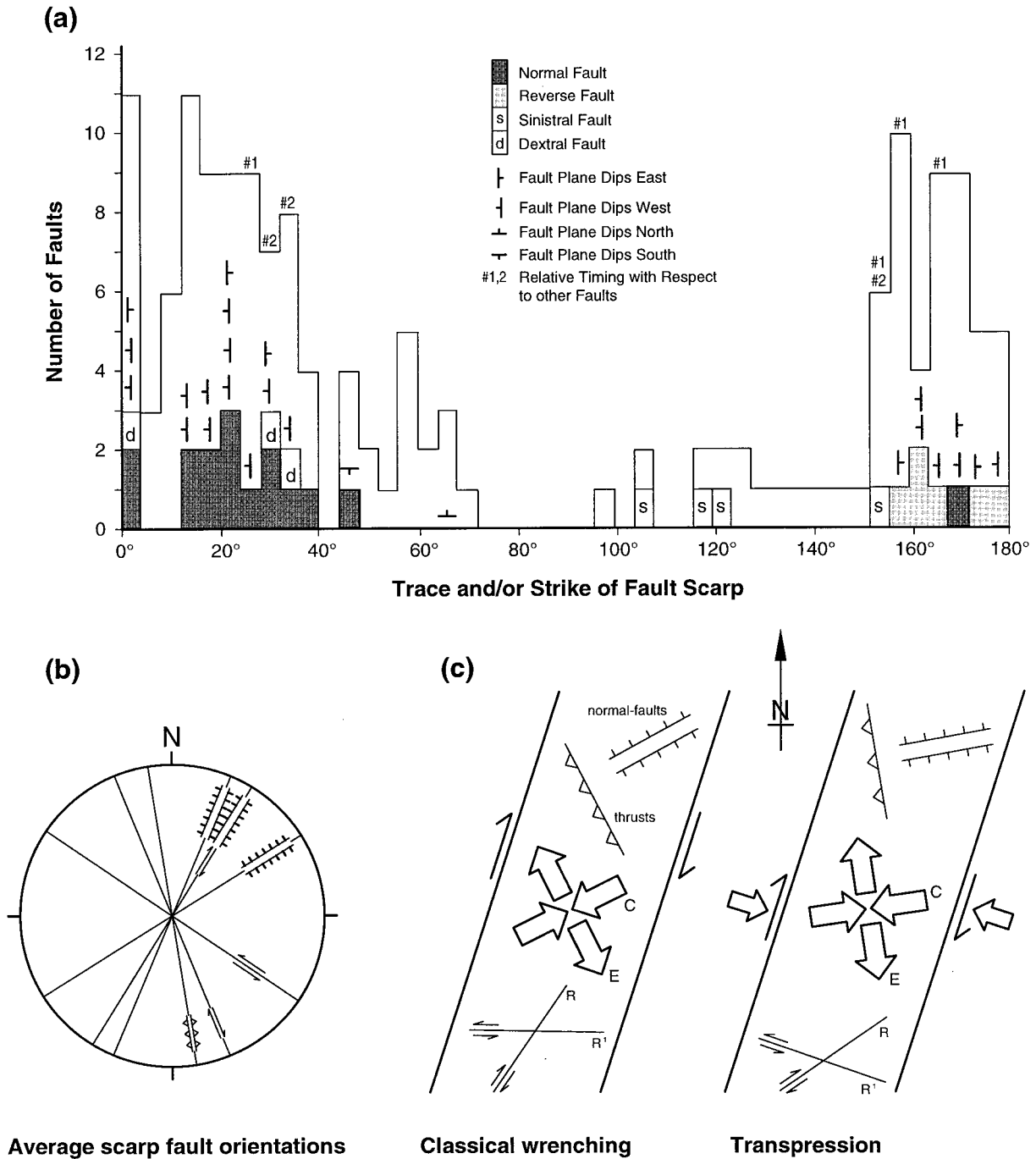


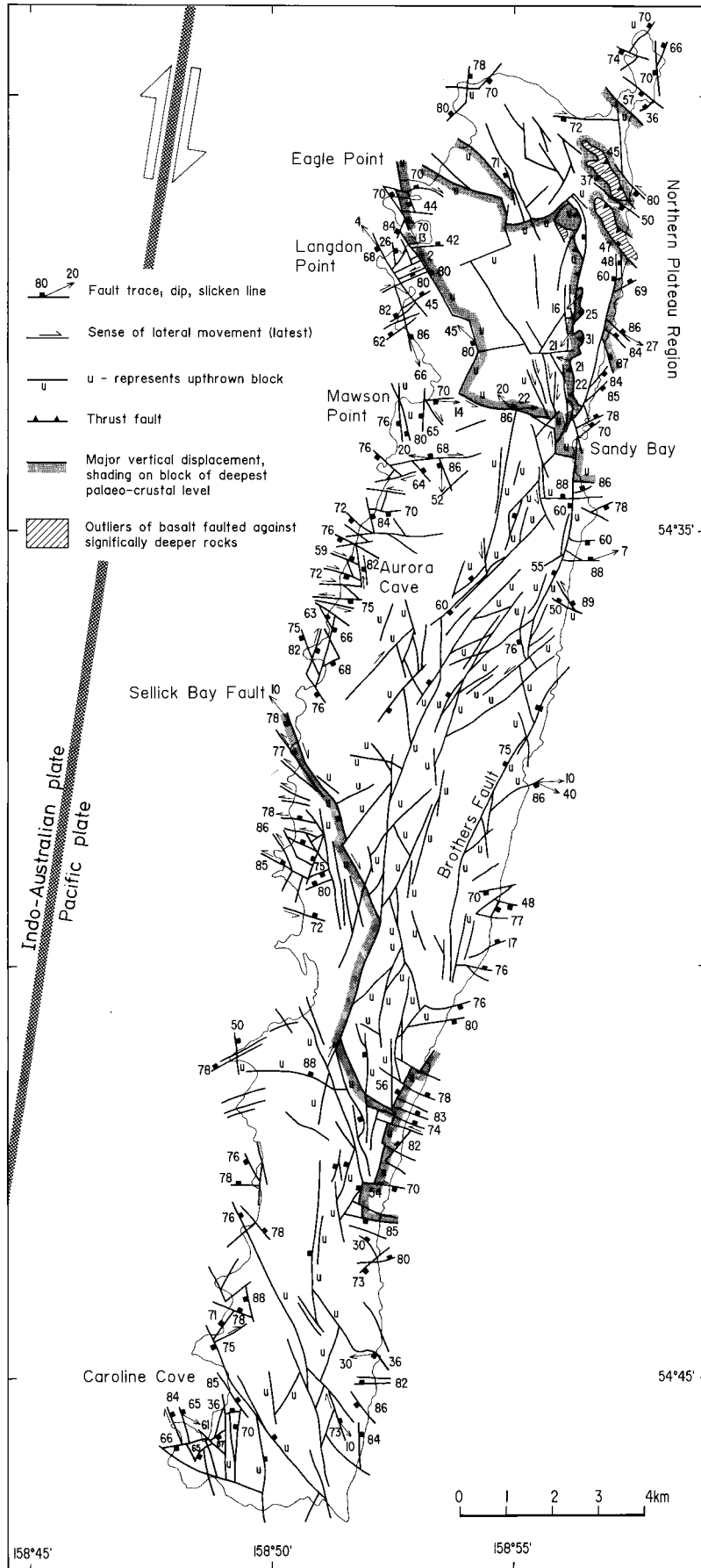
Fig. 15. (a) Frequency distribution of the trace orientations of neo-tectonic fault scarps and (b) average orientation distribution of neo-tectonic fault sets; (c) models of tectonic environment (after Sanderson and Marchini, 1984).

pre-date dry gouge-faults. Further, vein-faults form a broad spread in orientations centred on the mean orientation of D_1 dolerite dykes (App. A). These relationships suggest vein-faults are diagnostic of D_1 extensional tectonics, with only a minor proportion forming during D_3 .

10.4. Dry gouge-faults

Gouge-faults are sharp, straight to curvi-planar, largely

devoid of hydrothermal veins and are widespread, occurring in all rock associations. Widths range from 0.1 to 50 cm and average 5.5 cm; wider faults are classified as major faults (see below). Lateral displacements are greater than vein-faults, ranging from 0.2 cm to 50 m (averaging 2.42 m). Spatial density is high, with estimates of 115–700 gouge-faults/km², similar to vein-faults. In contrast, however, gouge-faults are heterogeneously distributed, with most in zones closely associated with major faults. The matrix is



tri-modal, being mostly very fine-grained foliated gouge containing sub-angular fragments of both 0.005–0.1 mm and 1–4 mm (10–30%) grainsize.

Three fault sets are recognized and these maintain similar orientations in all domains, suggesting formation during and/or subsequent to D_3 block rotations. The dominant set consists of dextral strike–slip faults of NNW- to NNE-strike and steep (70–80°) westerly dips; these are commonly reactivated by normal movement. Sinistral faults of 100° to –130°-strike and moderate (50–70°) SW or steep (60–80°) NE dips have SE- and NW-plunging slickenlines. A minor fault set of NE-strike and steep SE dips experienced oblique dextral/reverse movements along shallow to moderately NE-plunging slickenlines. These three fault sets are very similar to neotectonic fault scarps and entirely compatible with NE–SW to ENE–WSW shortening and D_3 dextral transpression. Gouge-faults formed throughout the evolution of Macquarie Island, but disproportionately during D_3 (Fig. 2), with 95% of gouge-faults post-dating dolerite dykes, hydrothermal retrogression and dilational foliations.

10.5. Neotectonic fault scarps

Recent faulting is evidenced by very common fault scarps confidently constrained to be younger than emergence of the island at 0.5 Ma (Adamson, personal communication, 1996) (Fig. 2). Most are significantly younger and offset palaeo-beach deposits (0.12–0.35 Ma; Adamson personal communication, 1996), palaeo-lake deposits (0.005–0.0135 Ma; Selkirk et al., 1988) and paths to penguin rookeries. Formation of scarps during recent earthquakes has been observed (Ledingham, 1978). Fault scarps are straight to curvi-straight, laterally extensive (km-scale) with 1–50 m throws. Where exposed in coastal platforms they comprise zones ≥ 50 cm wide containing numerous breccia- and gouge-faults dipping from 55° to 75°.

Four orientation sets are apparent (Fig. 15). NNE-striking dextral and normal fault scarps are the most common and typically youngest, with measured lateral displacements ranging from 80 m to 2.5 km. ENE-striking normal fault scarps and E- to SE-striking sinistral fault scarps are widespread. NNW-striking fault scarps have reverse movements and are typically the earliest formed. Neotectonic fault scarp orientations are consistent with dextral transpression at the Indo-Australian/Pacific plate margin, which in the vicinity trends parallel to the dominant NNE-striking scarps (Fig. 15). The conjugate set of sinistral and dextral faults constrain a shortening axis of 070°-trend which is normal to the reverse fault scarps (Fig. 15). ENE-directed shortening is consistent with recent earthquake focal mechanism solutions in the vicinity of the Central Macquarie Ridge (Fig. 1).

10.6. Major faults

Major faults are laterally extensive gouge and breccia zones of 30 cm–8 m width, often within a wider zone containing small-scale faults and fracture-cleavages which, in the upper-crust, are exclusively associated with and parallel to major faults (Figs. 8, 9, 16). Individual faults and fault networks delineate major changes in geology, juxtaposing different structural and/or rock association domains. Major displacements are inferred, with lateral displacements up to 2.5 km preserved in the neotectonic fault scarp record alone, and juxtaposed rock associations imply km-scale vertical displacements. Eleven major fault networks are recognized (Fig. 16) and can be grouped according to tectonic environment of formation, spanning D_1 growth faults to neotectonic fault scarps late in D_3 .

10.6.1. D_1 growth faults

The North Plateau is a mosaic of rock associations from different crustal levels (Figs. 3 and 16). Exposure of lower-crustal rocks on the North Plateau is primarily the result of early differential block uplift, with later modification by D_3 thrusts. Juxtapositions such as microgabbro/basalt, troctolite/sheeted dykes, harzburgite/sheeted dykes and harzburgite/basalt imply relative vertical displacements of >1.5, 2.75, >3 and 5.25 km, respectively (Goscombe and Everard, 1997, 1999). These juxtapositions resulted from differential block uplift accommodated by steep, bounding D_1 faults of NW- and WNW-strike (Fig. 16). These faults experienced early normal movements and were reactivated during D_3 by dextral strike–slip movements. After removal of D_3 block-rotation effects, major bounding faults had original strikes of 068–098°, which is consistent with formation as growth faults in the E-trending ridge segments of the PMSR.

Coarse gabbro clasts in talus deposits within the extrusive sequence at Langdon Point (Goscombe and Everard, 1997), imply that mid-crustal gabbros were exposed in a fault scarp with at least 2 km throw. Intra-volcanics talus deposits such as these constrain growth faults and differential uplift to very early in D_1 , while the volcanic pile was still forming (Goscombe and Everard, 1997). Furthermore, the presence of vertical dolerite dykes within tilted mantle lithosphere harzburgite, implies both tilting and uplift into mid-crustal levels occurred prior to D_1 dolerite dyke emplacement (Fig. 2).

10.6.2. D_3 thrust faults

Two low-angle thrusts are preserved on Macquarie Island, together comprising the Northeast Escarpment thrust

Fig. 16. Map of major faults (>30 cm wide). Note that fault traces on the central plateau are largely D_3 neo-tectonic fault scarps (because highly visible) and faults exposed in the coastal platforms are from all episodes of faulting from D_1 to D_3 . Poor outcrop on the plateau is responsible for the apparent low fault density. Approximate trace of Indo-Australian/Pacific plate margin after Schuur *et al.* (1998).

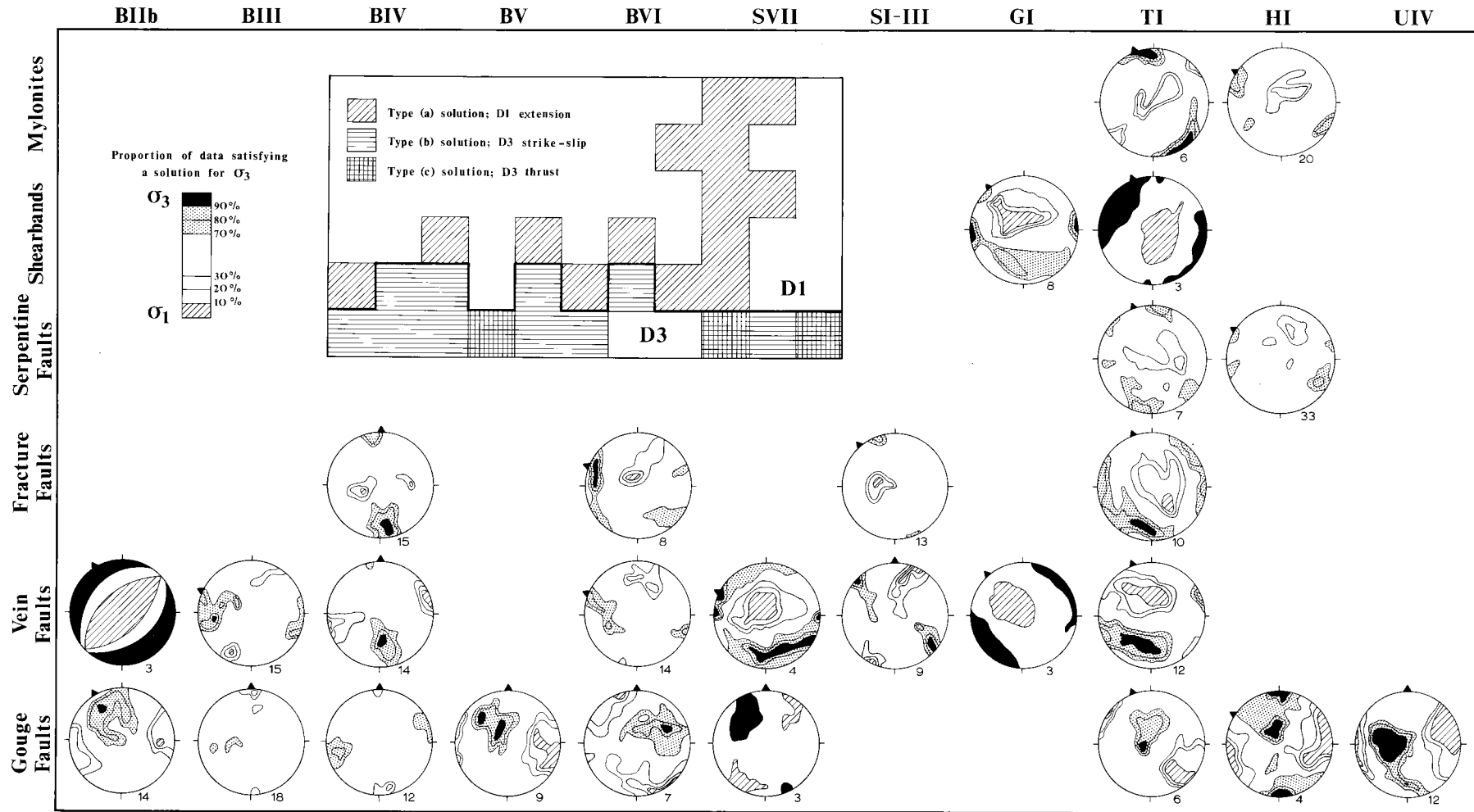


Fig. 17. Lower hemisphere equal area projection of results of palaeo-stress analysis of shear zone and fault populations by domain and grouped domains. Contours represent the percentage of the fault population that satisfy a solution for σ_3 . Palaeo-stress analysis by the method of Angelier and Mechler (1977) and solutions generated by the program EQUAL AREA JAN89 (Sorlein, 1989). Stereoplots are presented in their original orientation at the time of faulting (palaeo-north at top of page); back-rotated solutions are apparent where present-day north (black triangle) is oblique to palaeo-north. Inset outlines palaeo-stress solution type, which largely correlates with the fault episodes indicated.

system. Both involved SW over NE transport and are entirely compatible with the D_3 transpressional stress field. Two basalt domains on the northeast coast (BIIa and BIIb) are part of a dissected sheet that was thrust NE, onto sheeted dolerite dykes, along a sharp thrust plane dipping 30° to the SW (Figs. 4 and 16). Ultramafic and gabbro associations have been thrust on top of sheeted dolerite dykes along a well-exposed, 4 km long thrust at the eastern escarpment of the North Plateau (Figs. 4 and 16). The thrust zone is <5 m wide, dips 30° W and involved oblique reverse movements along slickenlines that plunge 20 – 30° to the SW. D_1 dykes and foliations are atypically shallowly inclined in the upper-plate, suggesting steepening of the thrust surface at depth.

10.6.3. Steep D_3 faults

The majority of major fault networks on the island are intimately associated with neotectonic fault scarps and formed during D_3 dextral transpression (Fig. 16). The Brothers Fault (Ledingham, 1978) is a network of NNE-, N- and NNW-striking faults and neotectonic scarps, stretching along the east coast from the north to south of Green Gorge (Fig. 16). These are steep (60 – 75°) W-dipping normal faults, up to 2.5 m wide, with dextral displacements of up to 1 km also recognized by displaced rock associations at Sandy Bay (Fig. 16). A network of steep, N- to NNE-striking faults and neotectonic fault scarps in the centre of the island experienced dextral displacements. These define the sharp boundary between BIII and BIVa structural domains, with a 65° angular discordance of the seafloor fabric (Fig. 11) indicating clockwise block rotation of BIII relative to BIVa during D_3 .

The Sellick Bay Fault is the most significant fault zone exposed on Macquarie Island (Fig. 16), with a breccia and gouge zone of 10 m width and a highly fractured deformation halo >50 m wide. The Sellick Bay Fault strikes 155° , dips steeply ($>70^\circ$) W and involved dextral movements along shallow NW-plunging slickenlines. This fault forms the northern boundary of the southern extrusives (BV and BVI), which are both stratigraphically distinct and of higher metamorphic grade than extrusives to the north (Goscombe and Everard, 1997, 1999). Dextral faults of 020° -strike have displaced the Sellick Bay Fault by up to 2.5 km (Fig. 16). The Sellick Bay Fault is parallel to palaeo-transform fracture zones in the vicinity of Macquarie Island, as demarcated on seafloor reflectivity and gravity images (Schuur et al., 1998).

10.7. Palaeo-stress analysis of faults and shear zones

Fault populations based on fault-type within specific structural domains, have been used for palaeo-stress analysis by the method of Angelier and Mechler (1977). All calculations were performed using the program EQUAL AREA JAN89 (Sorlein, 1989) (Fig. 17). Nearly all horizontal-axis tilting occurred very early in D_1 , thus palaeo-stress

results do not require back-tilting to remove these effects. However, D_3 block rotations around vertical axes must be considered when interpreting palaeo-stress results from all D_1 and some D_3 fault populations (Fig. 17). Three broad types of palaeo-stress solutions are recognized. Type (a) solutions have vertical σ_1 and horizontal σ_3 , characteristic of pure extension in a spreading ridge environment (Sykes, 1967). D_1 structures, such as ductile and semi-ductile shear zones, serpentine-fault, fracture-fault and some vein-fault populations, all have Type (a) solutions (Fig. 17). After back-rotation of D_3 effects, σ_3 axes have NW- to NNE-trend and are compatible with E- to ENE-trending ridge segments in the PMSR (Fig. 17).

All remaining solutions formed in compressional stress fields with horizontal to shallowly inclined σ_1 axes and σ_3 ranging between horizontal [Type (b)] and sub-vertical [Type (c)] (Fig. 17). Compressional solutions have only been recorded by gouge-faults and to a lesser degree by vein-fault populations and are correlated with movement events in D_3 . Nearly all compressional solutions are strike-slip [Type (b)], most with NE-trending σ_1 axes and few with N- or E-trending σ_1 (Fig. 17). Only solutions from the Northeast Escarpment thrust system (UIV) and gouge-faults from domains TI and BV, have thrust solutions [Type (c)], with NE- to SE-trending σ_1 axes (Fig. 17). Type (b) and (c) solutions are compatible with dextral strike-slip and transpression at the NNE-trending Central Macquarie Ridge (Fig. 1). Furthermore, these results and the predominance of strike-slip solutions, are identical to focal mechanism solutions from recent earthquakes in the Central Macquarie Ridge region (Frohlich et al., 1996; Fig. 1).

11. Thermal evolution of the lower-crust

Igneous crystallization assemblages, shear zone metamorphic assemblages and hydrothermal vein assemblages in faults and dilational fabrics, all document the temperature evolution of the lower crust, from the ductile to brittle fields, during D_1 (Fig. 18). Temperature conditions are estimated by comparison with experimental phase stability fields and by geothermometry (Appendix at end of paper (F)) based on mineral chemistry established by electron microprobe analysis (analytical details are available in the supplemental data files; App. E).

11.1. Ductile shear zones

Temperatures of crystallization of the host ultramafics are estimated by numerous geothermometers to be $1040 \pm 70^\circ\text{C}$ and $1053 \pm 73^\circ\text{C}$ in harzburgite and plagioclase-wehrlite, respectively (Appendix at end of paper (F)). These lower-crustal rocks cooled rapidly and experienced some brittle deformation (serpentine-faults and foliations, block tilting and uplift) prior to emplacement of gabbro dykes. Gabbro dykes crystallized at $944 \pm 84^\circ\text{C}$ (Appendix A) and were associated with a transient thermal perturbation

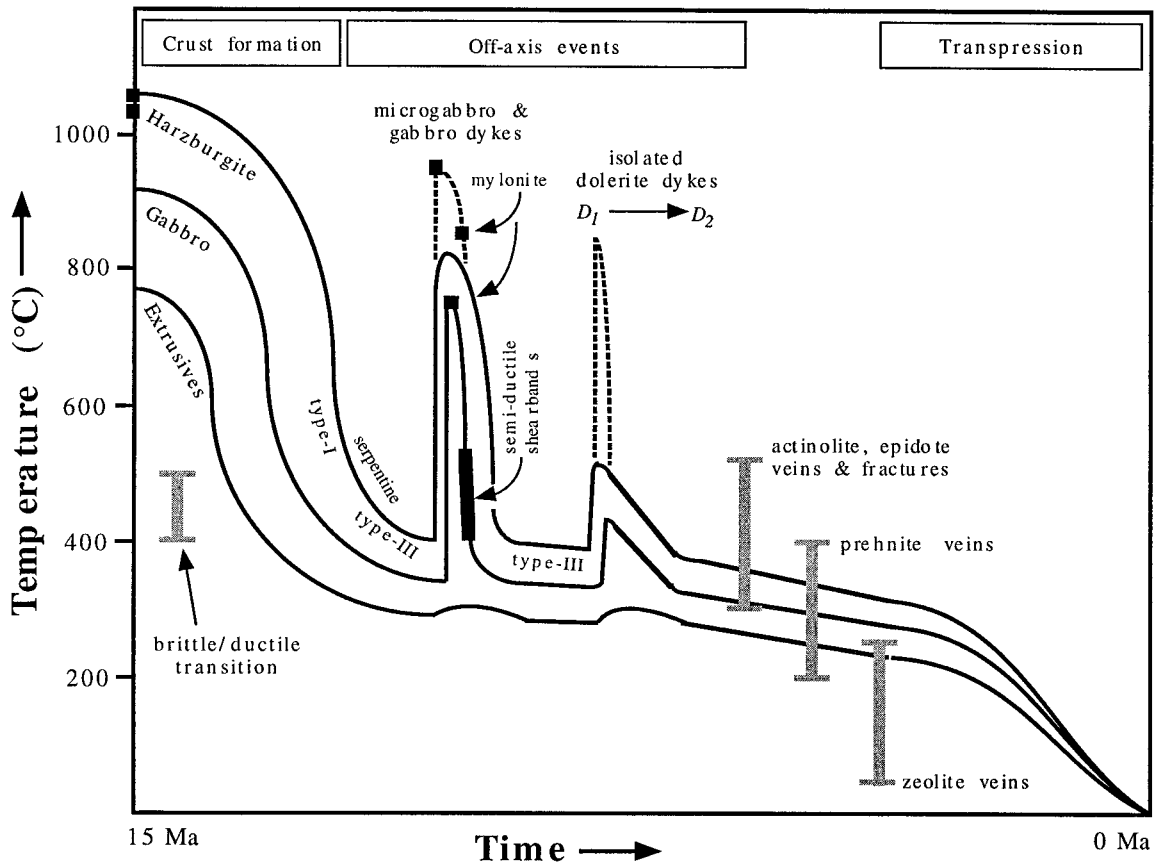


Fig. 18. Schematic and interpretive temperature–time curves for different crustal levels, including transient thermal perturbations due to periods of dyke emplacement (solid line) and within individual dykes (dashed). Temperature estimates based on geothermometry represented as solid square (see text; Appendix F) and temperature range of vein and fracture mineral phases as discussed in text.

as indicated by their coarse grainsize. During subsequent rapid cooling to a relatively cool ambient geotherm, ductile mylonites formed within the gabbro intrusions (Fig. 18). Mylonites in gabbro dykes have granulite facies assemblages of orthopyroxene–clinopyroxene–labradorite \pm edinitic hornblende \pm ilmenite, indicating conditions of formation of 760–920°C (Spear, 1981; Rong-long et al., 1986). This is further constrained by two-pyroxene geothermometry (Yamada and Takahashi, 1984; Finnerty and Boyd, 1987; Brey and Kohler, 1990), with results averaging $854 \pm 35^\circ\text{C}$ (Appendix F). Because of the fast cooling rate of individual dykes, re-equilibration during cooling is interpreted to be insignificant, preserving the temperature of mylonitization.

Ductile shear zones in the massive gabbro association formed relatively early, before the gabbro had cooled into the brittle field (Fig. 18). These mylonites and ultramylonites have assemblages of andesine–clinopyroxene–edenitic hornblende–ilmenite. The absence of orthopyroxene suggests mylonitization occurred at lower temperatures than in the gabbro dykes, at approximately 750–800°C (Spear, 1981). A single hornblende–plagioclase geothermometer (Holland and Blundy, 1994) result of

$762 \pm 50^\circ\text{C}$ (Appendix at end of paper (F)) is consistent with the phase stability field of this sample.

11.2. Semi-ductile shearbands

New mineral growth in semi-ductile shearbands include assemblages of chlorite–actinolite \pm epidote \pm plagioclase. Conditions of shearing are in the upper greenschist facies, at temperatures of 400–520°C (Liou et al., 1974; Bevens and Merriman, 1988; Begin, 1992; Spear, 1993). The earliest stages of shearing involved semi-ductile stretching of plagioclase and clinopyroxene and may have occurred at higher temperatures. These shear zones formed in the ductile/brittle transition, progressing from semi-ductile grain-refinement to brittle gouge development (Fig. 18). Associated late-stage vein assemblages are dominated by prehnite and rarely also contain chlorite, epidote, actinolite, zoisite and grossular, indicating temperatures of 300–400°C (Schiffman and Liou, 1980).

11.3. Brittle faults and dilational foliations

Serpentine-faults are dominated by clino-chrysotile and less commonly lizardite, whereas Type-III serpentine

veinlets are entirely chrysotile. These structures formed at conditions below 450–550°C, with lizardite suggesting possibly higher maximum temperatures of 650°C for some faults (Hemley et al., 1977; Wicks and O’Hanley, 1988). Conditions of <450–550°C confirm that brittle dilation of relatively cool ultramafic rocks occurred throughout most of D_1 , including prior to emplacement of gabbro dykes. Lizardite and magnetite constitute early, Type-I replacement of olivine at higher temperatures than the Type-III chrysotile-veinlets, which are largely devoid of magnetite (Moody, 1976).

Brittle, dilational foliations in gabbro, such as fractures and fracture-cleavages, contain actinolite \pm chlorite and formed at conditions spanning 300–520°C (Nitsch, 1971; Liou et al., 1974). Hydrothermal veins in the gabbro and ultramafic associations are dominated by prehnite and also contain actinolite, chlorite and zoisite indicating conditions of 300–400°C (Schiffman and Liou, 1980) and even lower for prehnite-only veins. Earliest episodes of veining contain epidote, forming at conditions spanning 300–550°C (Nitsch, 1971; Liou, 1973; Digel and Ghent, 1994) and rare xonotlite veins in harzburgite formed at approximately 300–425°C (Harker, 1964). Lower temperature fracturing and veining, such as in the zeolite facies, is not evident in the lower-crustal rock associations but common in the sheeted dolerite dykes and extrusives.

12. D_1 and D_2 extensional stress fields

The D_1 palaeo-stress field can be defined by the wide range in dilational and extensional structures developed on all scales. It is generally accepted that upper-crustal dykes in a spreading ridge environment strike sub-parallel to the spreading ridge and is one feature, along with fault scarps etc., that define the seafloor spreading fabric (Nicolas, 1989; Searle, 1992; Nicolas et al., 1994). The axis of maximum extension (σ_3 in a pure shear environment) is sub-horizontal and orthogonal to the seafloor spreading fabric at the time of its formation. This generally holds true, particularly in the extrusive domains where dykes were emplaced sub-vertically, as constrained by bedding indicators.

However, in mid- and lower-crustal rock associations, departures from this ideal geometry occur, but in all cases, σ_3 remains orthogonal to the dyke strike. In almost all domains, tilting was around a sub-horizontal axis parallel to the average dyke strike, leaving dyke strikes unchanged. In the lower-crust, dykes were often emplaced non-vertically, but with strikes parallel to other dilational features in the same domain. Conjugate dyke sets in the gabbro association (Fig. 7) formed with the σ_3 axis being the symmetrical bisector, orthogonal to the strike of both dyke sets. Other bi-modal dyke distributions in gabbros and troctolites (Figs. 6 and 7; App. A) are the result of one set being diagnostic of the regional stress field (i.e. originally

vertical) and the second (sub-parallel to compositional layering) in a local stress field generated by either the first dyke set (Hoek and Seitz, 1995) or low-angle extensional shear zones.

All D_1 intrusive events of gabbro, microgabbro and dolerite dykes have the same average strike within each structural domain (Figs. 6 and 7; App. A). Gross map-scale dilation, indicated by lateral transition zones between rock associations (Fig. 4), as well as small-scale D_1 structures such as shear zones, brittle faults and dilational foliations, have average strikes sub-parallel to the average D_1 dolerite dyke strike (Figs. 6 and 7; App. A). Thus the full spectrum of D_1 dilational and extensional structures are consistent with formation in the one extensional stress field, with the seafloor fabric best defined by D_1 dolerite dykes (Table 1).

Only domain BIVa still preserves a seafloor fabric (trending 080°) consistent with the E- to ENE-trending ridge segments during the latter episodes of spreading at the PMSR, based on plate reconstructions (Lamarche et al., 1997). Consequently, domain BIVa is interpreted to approximate the original orientation of the seafloor fabric in Macquarie Island crust. If other domains are back-rotated so that average D_1 dyke orientations are comparable to BIVa (Table 1), the original orientation of structures at the time of crust formation, prior to D_3 block rotations, is approximated. Back-rotated palaeo-stress solutions from D_1 structures such as mylonites, shearbands, fracture-faults, serpentine-faults and vein-faults, mostly have NNW- to NNE-trending σ_3 axes (Fig. 17) and are compatible with an E- to ENE-trending ridge segment. Back-rotated isolated D_2 dykes strike on average 134°, and the Sandell Bay Swarm 125° (Figs. 11(b) and 19; App. B). Consequently, D_2 involved palaeo-NE–SW extension, oblique by 45–54° with respect to the D_1 extension axis.

A minor orientation set of dilational structures (veins, fracture-cleavages and serpentine veinlets) normal to the seafloor fabric, is developed in lower-crustal associations (Figs. 6 and 7; App. A). These do not differ from, and are essentially coeval with, the dominant orientation set. This additional extension axis is inconsistent with pure extension at the spreading ridge and suggests also a component of along-axis extension at some stage during D_1 . Structures recording along-axis extension formed over a protracted middle- D_1 period, between gabbro and dolerite dyke events. Along-axis extension was most prevalent in mantle lithosphere harzburgite, suggesting drag on the lower crust by the mantle flow regime and implying along-axis as well as divergent mantle flow at the spreading ridge axis.

13. Post-crust formation extensional strain

Minimum estimates of crustal dilation (stretch), subsequent to initial crust formation, must consider the

Table 1

Summary of hypothetical vertical-axis block rotation and horizontal-axis tilting on Macquarie Island. Hypothetical vertical-axis rotation of domains assuming a palaeo-seafloor fabric originally coincident with BIVa (080°). Hypothetical horizontal-axis tilting of domains and sub-domains, assuming originally horizontal bedding/compositional layering and/or vertical dykes. All estimates based on average orientation of structures in each domain (Appendix A). NW Nth Plateau = TI, PI and PII; N Nth Plateau = GI, GII, SI, SII and UI; SW Nth Plateau = HI, SV, GIII and MII; SE Nth Plateau = SIII, MI and GIV; Lusi Swarm = SVIIa and SVIIb (Fig. 3).

Domain	Vertical-axis block rotation		Horizontal-axis tilting of domains and sub-domains			
	Rotation from BIVa	Seafloor fabric used	Tilting episode	Tilting axis ^a	Degree of tilting ^b	Tilting constrained by
<i>Upper-crustal extrusive domains</i>						
BI	35° clockwise	D_1 dolerite dykes	D_1 pre-dolerite dykes D_1 post-dolerite dykes D_1 total tilting ^c D_2 post- D_2 dolerite dykes	082° 082° 082° 125°	60° S 32° N 28° S < 46° NE	bedding & dolerite dykes dolerite dykes bedding & dolerite dykes bedding & dolerite dykes
BIIa	unknown	none	D_1 assumed	080° assumed	28° S	bedding
BIIb	6° anticlockwise	D_1 dolerite dykes	D_2 pre- D_2 dolerite dykes	143°	20° SW	bedding
BIII	65° clockwise	D_1 dolerite dykes	D_1 pre-dolerite dykes D_1 post-dolerite dykes D_3 syn/post-block rotation	095° 080° 030°	35° N & S 05° N 30° SE & NW	bedding dolerite dykes bedding
BIVa	0°	D_1 dolerite dykes	D_1 pre-dolerite dykes D_1 post-dolerite dykes	080° 080°	47° S & 13° N 10° N	bedding dolerite dykes
BIVb	20° clockwise	D_1 dolerite dykes	D_2 post- D_1 dolerite dykes	150°	23° NE	bedding
BIVc	47° clockwise	D_1 dolerite dykes	D_3 syn/post-block rotation	023°	28° NW	bedding
BVa + SVIIIa	68° clockwise	D_1 dolerite dykes	D_2 post- D_2 dolerite dykes	153°	19° NE	bedding & dolerite dykes
BVb + SVIIIb	68° clockwise	D_1 dolerite dykes	D_2 post- D_2 dolerite dykes	120°	44° NE	bedding & dolerite dykes
BVI	68° clockwise	D_1 dolerite dykes	D_1 pre-dolerite dykes D_1 pre-dolerite dykes	077° 102°	30° N 26° S	bedding bedding
<i>Mid-crustal sheeted dyke swarms</i>						
SI	42° clockwise	D_1 dolerite dykes	D_1 post-dolerite dykes	080°	34° N	dolerite dykes
SII	40° clockwise	D_1 dolerite dykes	D_1 post-dolerite dykes	080°	10° S & N	dolerite dykes
SIII + MI	20° clockwise	D_1 dolerite dykes	D_1 post-dolerite dykes	080°	59° N	dolerite dykes
MII	52° clockwise	D_1 dolerite dykes	D_1 post-dolerite dykes	080°	35° N	dolerite dykes
SV	63° clockwise	D_1 dolerite dykes	D_1 post-dolerite dykes	080°	32° S	dolerite dykes
MIII	90° clockwise	D_1 dolerite dykes	D_1 post-dolerite dykes	080°	66° S	dolerite dykes
SVIIa	65° clockwise	D_1 dolerite dykes	D_1 post-dolerite dykes	080°	60° N	dolerite dykes
SVIIb	65° clockwise	D_1 dolerite dykes	D_1 post-dolerite dykes	080°	13° N	dolerite dykes
<i>Lower-crustal intrusive domains</i>						
GI	40° clockwise	D_1 dolerite dykes	D_1 pre-microgabbro dykes D_1 pre-dolerite dykes D_1 post-dolerite dykes D_1 total tilting ^c	085° 085° 085° 085°	35° S 07° S 16° S 58° S	layering & gabbro dykes gabbro & dolerite dykes dolerite dykes layering
GII	37° clockwise	D_1 dolerite dykes	D_1 post-dolerite dykes	080°	35° N	dolerite dykes
GIII	55° clockwise	D_1 dolerite dykes	D_1 post-dolerite dykes	080°	24° N	dolerite dykes
GIV	33° clockwise	D_1 dolerite dykes	D_1 post-dolerite dykes	080°	54° N	dolerite dykes

Table 1 (continued)

Domain	Vertical-axis block rotation		Horizontal-axis tilting of domains and sub-domains			
	Rotation from BIVa	Seafloor fabric used	Tilting episode	Tilting axis ^a	Degree of tilting ^b	Tilting constrained by
TI	20° clockwise	D_1 dolerite dykes	D_1 post-gabbro dykes	080°	18° N	gabbro dykes
			D_1 pre- D_2 dolerite dykes	138°?	> 11° NE	layering & gabbro dykes
			D_1 total tilting ^c	080°	29° N	layering & gabbro dykes
PI	30° clockwise	D_1 dolerite dykes	D_1 pre-gabbro dykes	083°	02° S	layering & gabbro dykes
			D_1 pre-dolerite dykes	083°	11° S	layering & gabbro dykes
			D_1 post-dolerite dykes	083°	36° S	layering & gabbro dykes
			D_1 total tilting ^c	083°	49° S	layering
PII	16° clockwise	D_1 dolerite dykes	D_1 pre-dolerite dykes	090°	39° S	layering & dolerite dykes
			D_1 post-dolerite dykes	090°	19° S	dolerite dykes
			D_1 total tilting ^c	090°	58° S	layering
UIV	47° clockwise	D_1 dolerite dykes	D_1 pre-gabbro dykes	093°	20° S	layering & gabbro dykes
			D_1 pre-dolerite dykes	093°	51° S	gabbro & dolerite dykes
			D_1 post-all dykes	093°	51° N	layering & dolerite dykes
			D_1 total tilting ^c	093°	20° S	layering
HI	58° clockwise	D_1 gabbro dykes	D_1 pre-all dykes	124°	46° NE	layering & all dykes
	79° clockwise	D_1 dolerite dykes	D_1 pre-all dykes	103°	46° N	layering & all dykes
HII + HIII + UIII	10° clockwise	D_1 dolerite dykes	D_1 pre-dolerite dykes	097°	62° S	layering & dolerite dykes
			D_1 post-dolerite dykes	097°	26° N	dolerite dykes
			D_1 total tilting ^c	097°	36° S	layering
<i>Averages for grouped intrusive domains on the North Plateau and in the Lusi Swarm</i>						
NW Nth Plateau	22° clockwise		D_1 total tilting ^c	084°	45° N & S	
N Nth Plateau	40° clockwise		D_1 total tilting ^c	081°	32° N & S	
SW Nth Plateau	37° clockwise		D_1 total tilting ^c	086°	34° N & S	
SE Nth Plateau	27° clockwise		D_1 total tilting ^c	080°	57° N	
Lusi Swarm	65° clockwise		D_1 total tilting ^c	080°	46° N & S	

^a Tilting axes are back-rotated to remove effects of D_3 block rotations.

^b Sense of tilting defined by direction of movement of top of bed or dyke. Incremental tilting history in some domains is read down the page.

^c An alternative scenario of tilting constrained by bedding/layering only and dykes emplaced non-vertically.

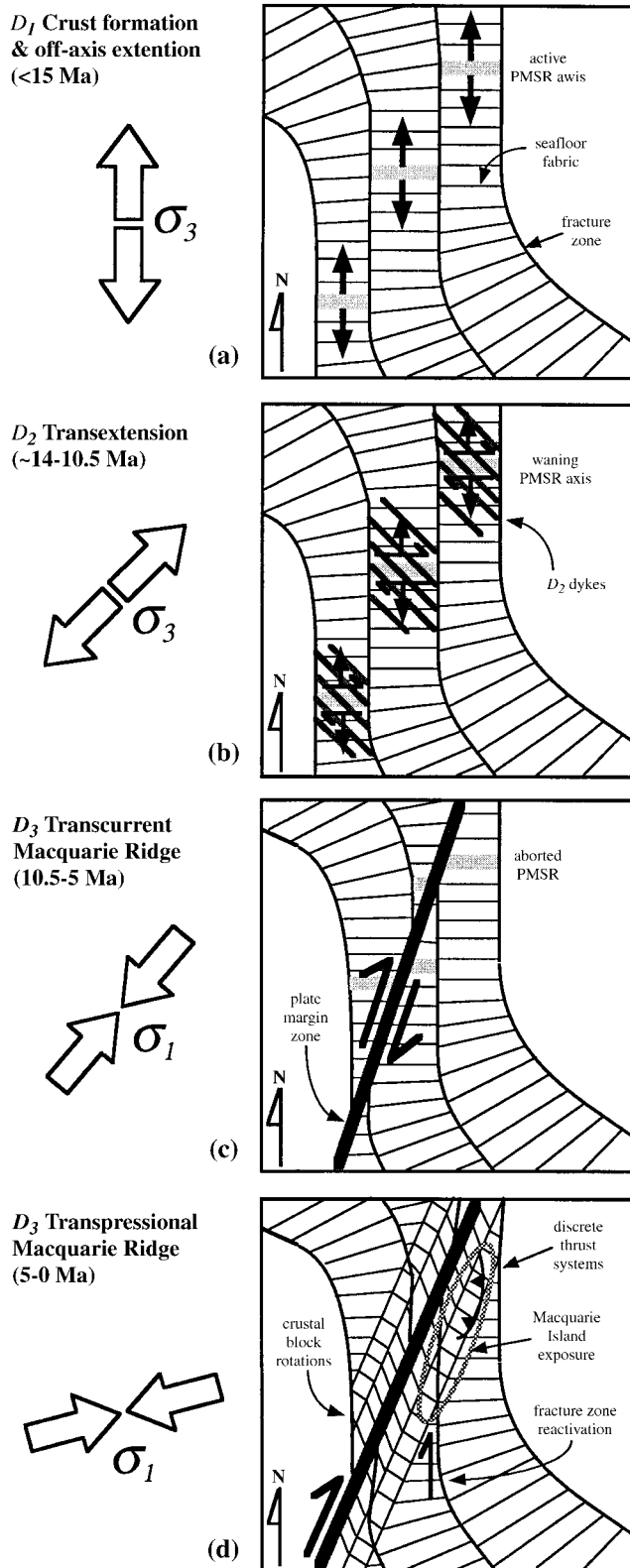


Fig. 19. Schematic representation of the evolution of the tectonic stress field in the vicinity of Macquarie Island. (a) Crust generation and extension at the PMSR during D_1 . (b) D_2 transextension, a transitional period of plate reorganization. (c) Initiation of the transcurrent Indo-Australian/Pacific plate margin (D_3) as a dextral strike-slip system that evolved into a transpressional plate margin (d), that has persisted to the present day. North at top of page.

accumulative strain partitioned between a wide range of deformational and intrusive structures. Total accumulative dilation decreases markedly up through the crustal profile. Up to 44% dilation in the harzburgites was contributed by gabbro dykes (<24%), serpentine veinlets (<8%), serpentine-faults (<7%) and only 5% by dolerite dykes (App. D). The other ultramafic associations experienced up to 38% dilation, this being mostly due to copious dolerite dykes (21–35%). In the gabbro association, total dilation up to 12.5% is due mostly to dolerite dykes (3.5–10.5%) and a minor component from fractures, shear zones and micro-gabbro dykes (2%). Dolerite dykes accommodated only 1.3–3.3% dilation in extrusives, with a possibly greater, unestimated proportion due to veins, fractures, fissures and normal growth faults.

Crustal extension due to D_1 dolerite dykes is estimated from average dyke width, inclination and spatial density along sections and within entire domains (App. D). Total minimum crustal extension accompanying isolated D_1 dolerite dykes for the whole island is calculated at 3.6% (App. D). In the upper crust, this is heterogeneously partitioned across the island: ranging from 1.3 to 1.4% in the south (BIVb, BIVc, BV and BVI) to 3.2–3.3% in the centre (BIII and BIVa), with sub-domains up to 15% (App. D). D_1 strain partitioning is similarly reflected by lower density of veining and faulting in the south. Isolated D_2 dolerite dykes constitute only 0.5% extension across the island and a total of 2.6% with the Sandell Bay Swarm included (App. D). In contrast to D_1 , D_2 dilation is largely partitioned into the southern extrusive domains (BV and BVI).

14. Tilting around horizontal axes

Two classes of block rotation are recognized on Macquarie Island: tilting of domains and sub-domains around horizontal axes, predominantly during D_1 and D_2 , and rotation of crustal blocks around vertical axes during D_3 . The entire spectrum of domain average orientation data (App. A) can be rationalized in terms of these two rotation axes. Being about mutually orthogonal axes, these two block rotations can be analysed independently of each other. The degree of tilting (Table 1) around a horizontal axis (strike of the tilted structure) is quantified by assuming originally horizontal bedding/compositional layering and vertical dykes (Nicolas, 1989; Searle, 1992; Nicolas et al., 1994). These assumptions are generally true in extrusives, where dykes in all domains are sub-orthogonal to bedding defined by flattened pillows, tabular lava flows and sedimentary units.

Many lower-crustal domains have inclined compositional layering and vertical dykes, indicating tilting soon after crust formation and prior to dyke emplacement. With multiple dyke events (gabbro, microgabbro and dolerite dykes), a history of incremental tilting can be documented,

assuming dykes of each event were emplaced vertically (Table 1). Four episodes of tilting are recognized: early D_1 tilting prior to dolerite dyke emplacement; tilting subsequent to D_1 dolerite dykes during both D_1 and D_2 ; and rare D_3 tilting (Table 1).

14.1. Early D_1 tilting

Most extrusive domains have bi-modal bedding distributions of similar but opposing average dips (23–37°) (Fig. 9). Sub-domains with constant dip direction are 20–2000 m wide across strike (Fig. 11). Alternating bedding inclination is not due to open folding as a continuous profile plane distribution is not apparent (Fig. 9) and no folding on any scale is recognized on Macquarie Island. The bi-modal bedding distribution is due to either tilting away from the spreading ridge during normal faulting (Sykes, 1967) and/or an earlier phase of tilting towards the ridge during flexure and subsidence off the ridge axis (Rosencrantz, 1982). An interrelated process, here termed ‘pseudo-tilting’, is eruption of tabular lavas and flattened pillows onto an already inclined seafloor, this ‘bedding’ preserving the orientation of the palaeo-slope. Inclined palaeo-slopes originate from either early (accompanying eruption of extrusives) real-tilting of the seafloor surface and/or slopes generated by eruption from fissures, both resulting in the same bedding distribution.

Dykes and bedding in extrusives have sub-parallel strikes (Table 1; App. A), and are thus consistent with both down-slope eruption away from ridge-parallel fissures and tilting of the seafloor accompanying normal faulting in the spreading ridge environment. Dolerite dykes are vertical in extrusive domains, indicating that inclined bedding pre-dated the isolated dolerite dykes and must be an artefact of original crust formation in a spreading ridge environment. ‘Pseudo-tilting’ cannot be discounted because tabular lavas and flattened pillows constitute 82% of ‘bedding’ data and significantly weight the bedding distributions (Fig. 9). However, co-planar tabular lavas and sedimentary units are documented, implying true-tilting occurred subsequent to lava extrusion. Early D_1 tilting is further illustrated by local angular unconformities with intra-volcanic talus and turbidity flow deposits, over-lying lavas with steeper bedding (Goscombe and Everard, 1997).

Most lower-crustal rock associations with compositional layering experienced total accumulative tilting of 20–58° towards the south, around back-rotated axes of 080–097° trend (Table 1). These tilting axes are sub-parallel to the seafloor fabric in PMSR segments and entirely consistent with D_1 tilting in a spreading ridge environment. Predominance of tilting towards the south implies N-dipping growth faults for a slow- or intermediate-rate spreading ridge (Searle, 1992; Carbotte and Macdonald, 1990), and a ridge axis to the north, implying that Macquarie Island rocks were generated in the Pacific plate (Fig. 19). Nearly all tilting of lower-crustal rock associations occurred

early in D_1 , prior to emplacement of sub-vertical dolerite dykes (Table 1; App. A). Only in harzburgite (HI) did all tilting occur prior to both gabbro and dolerite dykes. Domains GI, PI and PII involved two tilting increments, both with the same vergence: 13–42° prior to dolerite dykes (most being also prior to micro-gabbro dykes) and late- D_1 tilting of 16–36° subsequent to dolerite dykes (Table 1).

14.2. Late D_1 tilting

D_1 tilting subsequent to dolerite dyke emplacement, is recognized in only three extrusive domains: 5–10° in BIII and BIVa and 32° in BI. Few lower-crustal domains experienced late D_1 tilting, averaging only 24° (Table 1). Total D_1 tilting of sheeted dolerite dyke domains, assuming vertical emplacement, averages 37° which is typical of total D_1 tilting in other associations (Table 1). By comparison to lower-crustal associations, tilting of sheeted dolerite dykes is interpreted to have occurred predominantly in early D_1 . Total accumulated D_1 tilting increases with crustal depth, averaging 28° in extrusives and 37°, 43° and 40° in sheeted dykes, gabbros and ultramafics, respectively.

14.3. D_2 tilting

D_2 tilting of sub-domains, around back-rotated axes of 120° to 153° trend, is only recognized in the extrusive domains BIVb, BVa, BVb and BVI and possibly BIIIb (Fig. 11; Table 1). The D_2 Sandell Bay dyke swarm is tilted in sympathy with bedding in domains BVa and BVb, around an axis parallel to the swarm (Figs. 8, 9, 11). Degree of D_2 tilting averages 29° and is consistently towards the NE (Table 1). The southwestern third of the island has been tilted predominantly by D_2 effects (Fig. 11), consistent with the high proportion of D_2 strain indicated by the predominance of D_2 dykes.

14.4. D_3 tilting

Tilting of bedding around back-rotated axes of 165–170° trend is recognized in domain BIVc and sub-domains within BIII (Table 1). Such tilting is consistent with ENE-shortening and may have occurred synchronously with D_3 vertical-axis block rotation. Sub-vertical and slightly over-turned sedimentary units are recognized within and adjacent to major D_3 fault zones at Langdon Point, Caroline Cove, Eagle Point and Aurora Cave (Fig. 16). Tilting was around axes trending 160–180° and occurred during D_3 crustal shortening within these fault zones. Domains UIV and HII, record a hypothetical tilting history of 62–71° prior to dolerite dyke emplacement and a later 26–51° tilting in the opposite direction (Table 1). These domains constitute the only D_3 thrust slivers on the island (Figs. 3 and 16), and this tilting history is compatible with D_1 tilting followed by back-rotation during D_3 over-thrusting.

15. D_3 block rotations around vertical axes

The seafloor fabric is defined by dolerite dykes (and in some domains gabbro dykes), which are generally considered to have been emplaced sub-parallel to the spreading ridge (Nicolas, 1989; Searle, 1992; Nicolas et al., 1994; Fig. 11; Table 1). Large (km-scale), fault-bounded crustal blocks on Macquarie Island have marked angular discordance of the seafloor fabric between them (Fig. 11), resulting from rotation around sub-vertical axes. Block rotation is quantified with respect to the least-rotated domain (BIVa), which preserves a 080°-trending seafloor fabric (Table 1) that is consistent with E- to ENE-trending ridge segments at the latter stages of the PMSR (Lamarche et al., 1997; Schuur et al., 1998).

Block rotations, with respect to BIVa, range from 6° to 68° and almost all are clockwise (Table 1). Block rotation is highest on the west coast, closest to the Indo-Australian/Pacific plate margin (Fig. 16) and is consistent with dextral transcurrent movement at this plate margin (Fig. 19). Block rotation on the island can be divided into 11 distinct domains and grouped domains (Table 1). Grouped domains on the North Plateau experienced rotations averaging 40° in the north, 57° in the southwest, 27° in the southeast and 22° in the northwest (Table 1). Domains BI, BIII, BIVb and BIVc experienced rotations of 35°, 65°, 20° and 47°, respectively. The southwestern third of the island, bounded by the Sellick Bay Fault, experienced the greatest block rotation, averaging 65–68°. This is further supported by palaeo-magnetic data indicating 55° clockwise rotation of the southern part of the island with respect to the north (Williamson, 1988).

Block rotation with respect to adjacent domains is almost entirely within the range 17–28° and averages 22°. This narrow range of inter-domain rotation suggest a mechanical limitation to block rotation as found in the similar scenario of mega-scale kinking (Goscombe et al., 1994). The domain that experienced highest relative rotation (BIII) also displays the broadest spread in D_1 dyke orientation (Fig. 10), suggesting a mosaic of variably rotated sub-domains that together contributed to the high degree of whole-block rotation.

Crustal block rotation is accommodated by both slip along the major bounding faults and internal deformation, apparently without folding, leading to progressive change in the shape (elongation and flattening) of the crustal block. The latter mechanism is akin to deformation in the internal zone of a kinkband, where strain is accommodated by slip along the cleavage planes (Goscombe et al., 1994). Macquarie Island rocks are unfoliated, but nevertheless, high degrees of internal strain can be accommodated by dextral strike-slip reactivation of small-scale D_1 faults and fractures. The high spatial density of these structures and evidence for strike-slip reactivation support such a mechanism. New gouge-faults initiated during D_3 have a

high spatial density and involved dextral strike-slip movements, consistent with accommodation of strain within a clockwise-rotated block.

Angular discordance (averaging 44°) of the seafloor fabric between sharply bounded elongate crustal blocks is evident in seafloor reflectivity images in the vicinity of the Central (Schuur et al., 1998) and North (Wood et al., 1996) Macquarie Ridge. These crustal blocks are restricted to within 35 km of the plate margin, involved clockwise rotation of an originally E-trending seafloor fabric, and are entirely consistent with dextral transpression at the Indo-Australian/Pacific plate margin (Fig. 19). In this block rotation zone, palaeo-transform fracture zones form some of the boundaries between rotated blocks and were presumably reactivated by dextral strike-slip. The Sellick Bay Fault on Macquarie Island is interpreted to be one such reactivated fracture zone (Figs. 16 and 19).

16. Discussion and conclusions

16.1. Tectonics in the spreading ridge environment (D_1)

D_1 was a protracted period of extensional tectonics encompassing initial crust formation and later intrusive events, a wide variety of extensional and dilational structures and accompanying hydrothermal veins and alteration in a near- to off-axis environment. Newly formed crust experienced tilting of 20–58° in mid- and lower-crust and 20–35° in upper-crust domains, very early in D_1 , mostly prior to emplacement of gabbro and dolerite dykes. Normal growth faulting in the spreading ridge environment was responsible for both tilting and km-scale differential block uplift and exposure of lower-crustal rocks in fault scarps.

Protracted brittle dilation in the lower- and mid-crust occurred from very early in D_1 and spanned successive intrusive episodes of coarse gabbro dykes, microgabbro dykes and dolerite dykes. All D_1 intrusive, dilational and deformational structures indicate formation in a pure extensional stress field with horizontal σ_3 and sub-vertical σ_1 . After removal of D_3 block rotation effects, an N-trending σ_3 axis is documented throughout the entire D_1 period and in all domains. This is consistent with formation at an E-trending spreading ridge segment of the PMSR (Fig. 19). Crustal extension subsequent to crust formation, in the near-axis environment, was considerable and accommodated largely by dykes and also dilational and extensional structures. Estimates of crustal extension, not including growth faults, decreased markedly up through the crustal pile, being <44%, <38%, <12.5% and 1.3–3.3% in the harzburgite, ultramafics, gabbro and extrusive associations, respectively.

A subsidiary extension direction, orthogonal to the dominant extension direction, is also recorded by some D_1

structures in the lower crust. This along-axis extension occurred throughout a protracted period from prior to gabbro dykes up to emplacement of dolerite dykes and was greatest in the mantle lithosphere harzburgite, suggesting drag on the lower lithosphere by flow in the asthenosphere. This implies a complex mantle flow pattern at the spreading ridge, involving both divergent flow away from the ridge and flow along the ridge axis away from mantle diapirs, as documented in the Oman ophiolite (Nicolas, 1989; Nicolas and Boudier, 1995) and the Trinity complex (Boudier et al., 1989).

In the lower-crust, pervasive dilational structures formed in the brittle field (below 450–550°C) throughout most of D_1 , including both prior to and after gabbro dykes (Fig. 18). Ductile deformation was entirely localized within gabbro dykes (at 850°C) and rare, thin shear zones in the gabbro association (at 750–800°C). A transient brittle/ductile transition (400–520°C) is recorded by semi-ductile shearbands in the basal gabbro and troctolite associations (Fig. 18). Pervasive ductile deformation of the harzburgite and ultramafic associations is not evident in outcrop nor thin section. This is in stark contrast to many ophiolite terranes where harzburgites preserve L – S grain-shape fabrics in olivine and stretched spinel and pyroxene grains (Girardeau and Nicolas, 1981; Salisbury and Christensen, 1985; van der Wal et al., 1992; Nicolas and Boudier, 1995), formed by plastic, high-temperature, low-stress flow in the asthenospheric mantle (Nicolas, 1989; Cannat et al., 1992).

16.2. Tectonics during D_2

A second extensional stress field (D_2) immediately post-dates D_1 and involved limited palaeo-NE–SW crustal extension. D_2 was expressed as late-stage dolerite dykes of 124–159°-strike, including the Sandell Bay Swarm, late-stage hydrothermal veins sub-parallel to D_2 dykes and tilting around SE-trending axes in domains BI, BIVb, BV and BVI. Possible D_2 extrusives include pillows erupted from a 146°-striking fissure; these constitute the youngest volcanics on Macquarie Island, while sub-horizontal lavas at Mawson Point overlie a local unconformity and are devoid of D_1 dolerite dykes (Fig. 11). D_2 extensional strain was greatest in the southwestern third of the island (BV and BVI). D_2 strain was small (2.6% extension in total) and either did not involve a new spreading ridge axis and generation of new crust, or Macquarie Island crust was sufficiently distant to be little affected.

The D_2 extensional stress field formed at some stage during transition from a spreading ridge environment (D_1), to a dextral transcurrent plate margin (D_3). Concurrent dilation and dextral strike–slip movements at 080°-trending ridge segments in the PMSR would have resulted in an approximately NE–SW trending σ_3 axis (Fig. 19). Consequently, a period of transtension during plate reorganization at the latter stages of D_1 and

before initiation of the transcurrent plate margin proper (D_3), may be responsible for the D_2 stress field. Plate reconstructions suggest a period of coeval crustal extension and strike–slip movements at 14–10.5 Ma (Molnar et al., 1975).

16.3. Transpressional tectonics at the Macquarie Ridge (D_3)

Extensional tectonics in the PMSR was terminated by dextral transcurrent movements, with onset of the present style of Indo-Australian/Pacific plate margin at approximately 10.5 Ma (Molnar et al., 1975). This plate margin has evolved progressively from a strike–slip margin to a transpressional margin (Frohlich et al., 1996; Fig. 19). Palaeo-stress analyses of D_3 gouge- and vein-fault populations have mostly strike–slip solutions with a NE-trending σ_1 . The geometry of neotectonic fault scarps is also consistent with dextral transpression and NE-trending σ_1 (Fig. 15). The Northeast Escarpment thrust system and rare palaeo-stress thrust solutions, attest to discrete episodes of compressional tectonics during D_3 . These findings are consistent with focal mechanism solutions of recent earthquakes in the vicinity of Macquarie Island (Fig. 1; Frohlich et al., 1996).

Dextral transpression at the Indo-Australian/Pacific plate margin was accommodated by strike–slip movement at both the highly sheared, 1–5 km wide plate margin zone (Schuur et al., 1998) and sub-parallel fault networks (expressed on Macquarie Island), and vertical-axis rotation of fault-bounded crustal blocks within 35 km of the plate margin (Fig. 19). All block rotations are clockwise, increase in amount towards the west (range up to 68°) and are entirely consistent with dextral transpression at the plate margin 3–5 km to the west of the island (Fig. 16). Internal strain within rotated crustal blocks is accommodated by strike–slip reactivation of small-scale D_1 faults and fractures, all of which have high spatial density on Macquarie Island.

Acknowledgements

All the staff of Mineral Resources Tasmania are gratefully acknowledged for support throughout this project. Encouragement by Drs Tony Crawford, Mike Coffin and Martin Hand and the constructive reviews of Drs Mike Rubenach, Rupert Sutherland and Richard Norris were greatly appreciated. Drs Tony Brown, Rick Varne, Tony Crawford and Pat Quilty initiated this project, with funding from the Australian Antarctic Foundation and ANARE. The support and encouragement of the 1994–1996 expeditioners, Mary-Anne Lea, Mark Hindell, Clive McMahon, Louise Wynen, Rags Raymond, Kiwi, Jeroen Creuwels, Simon Goldsworthy and Craig Tweedie, was inspirational, sincerely appreciated and a lot of fun.

Appendix

Geothermometry of gabbroic and ultramafic intrusives and shear zones on Macquarie Island (known as Appendix F)

Sample	Rock-type	T result (°C)			Geothermometer calibration
		2kb	4kb	6kb	
Harzburgite (HI and UIV)					
MQ397	opx-cpx-ol-sp		1121		opx (Witt-Eickschen and Seck, 1991)
			1065		opx-ol-sp (Witt-Eickschen and Seck, 1991)
		1049	1061	1073	ol-cpx (Powell and Powell, 1974)
		959	963	967	ol-sp (Ballhaus et al., 1991)
		720	720	721	opx-cpx (Finnerty and Boyd, 1987)
		713	715	717	opx-cpx (Yamada and Takahashi, 1984)
		842	844	847	opx-cpx (Brey and Kohler, 1990)
CH ^a	opx-cpx-ol-sp		992		opx (Witt-Eickschen and Seck, 1991)
			994		opx-ol-sp (Witt-Eickschen and Seck, 1991)
			1134		opx-ol (Podvin, 1988)
		1058	1070	1081	ol-cpx (Powell and Powell, 1974)
		1042	1046	1050	ol-sp (Ballhaus et al., 1991)
		846	846	847	opx-cpx (Finnerty and Boyd, 1987)
		839	841	844	opx-cpx (Yamada and Takahashi, 1984)
		940	943	945	opx-cpx (Brey and Kohler, 1990)
G1089(iii)	opx-cpx-ol-sp		1128		opx-ol (Podvin, 1988)
		1141	1122	1104	ol-cpx (Powell and Powell, 1974)
		985	988	991	ol-sp (Ballhaus et al., 1991)
Plagioclase–wehrlite (PI and UIV)					
MQ78	cpx-ol-sp-pl	1022	1034	1046	ol-cpx (Powell and Powell, 1974)
		957	959	962	ol-sp (Ballhaus et al., 1991)
MQ171	cpx-ol-sp-pl-ilm	1031	1047	1063	ol-cpx (Powell and Powell, 1974)
MQ907	cpx-ol-sp-pl	1022	1034	1046	ol-cpx (Powell and Powell, 1974)
		998	1001	1004	ol-sp (Ballhaus et al., 1991)
G1046D	cpx-ol-sp-pl	1184	1187	1190	ol-cpx (Kawasaki and Ito, 1994)
		1133	1136	1139	ol-sp (Ballhaus et al., 1991)
Olivine–gabbro (GI)					
G21A	cpx-ol-pl	1023	1026	1029	ol-cpx (Kawasaki and Ito, 1994)
Gabbro dykes and veins within harzburgite (HI)					
G72D	opx-ol-pl-phl		1060		opx-ol (Podvin, 1988)
G75E	cpx-opx-pl	824	824	825	opx-cpx (Finnerty and Boyd, 1987)
		812	814	816	opx-cpx (Yamada and Takahashi, 1984)
		857	859	862	opx-cpx (Brey and Kohler, 1990)
G72H	cpx-ol-pl-phl	1140	1143	1146	ol-cpx (Kawasaki and Ito, 1994)
G96B	cpx-opx-pl	962	963	964	opx-cpx (Finnerty and Boyd, 1987)
		950	953	956	opx-cpx (Yamada and Takahashi, 1984)
		947	949	952	opx-cpx (Brey and Kohler, 1990)
G107A(i)	cpx-ol-(pl)	998	1001	1003	ol-cpx (Kawasaki and Ito, 1994)
G107B	cpx-opx-pl	967	968	969	opx-cpx (Finnerty and Boyd, 1987)
		955	958	960	opx-cpx (Yamada and Takahashi, 1984)
		924	927	929	opx-cpx (Brey and Kohler, 1990)
G688	cpx-opx-ilm	918	919	919	opx-cpx (Finnerty and Boyd, 1987)
		906	909	911	opx-cpx (Yamada and Takahashi, 1984)
		916	918	920	opx-cpx (Brey and Kohler, 1990)
Mylonite zones in gabbro dykes and veins within harzburgite (HI)					
G72H	ol-opx-cpx-hn-pl	801	803	805	ol-cpx (Kawasaki and Ito, 1994)
			~ 770		hn-opx (Perchuk et al., 1985)
			~ 850		bi-cpx (Perchuk et al., 1985)
		817	817	818	opx-cpx (Finnerty and Boyd, 1987)
		805	807	809	opx-cpx (Yamada and Takahashi, 1984)
		686	688	690	opx-cpx (Brey and Kohler, 1990)
G72D	ol-opx-hn-pl	757	764	771	hn-pl (Holland and Blundy, 1994)
			~ 900		hn-opx (Perchuk et al., 1985)

(continued)

Sample	Rock-type	T result (°C)			Geothermometer calibration
		2kb	4kb	6kb	
G75E	opx-cpx-hn-pl-ilm		~ 790		hn-opx (Perchuk et al., 1985)
		848	849	850	opx-cpx (Finnerty and Boyd, 1987)
		837	839	841	opx-cpx (Yamada and Takahashi, 1984)
		760	762	764	opx-cpx (Brey and Kohler, 1990)
G80A(ii)	opx-cpx-hn-pl	778	783	789	hn-pl (Holland and Blundy, 1994)
			~ 830		hn-opx (Perchuk et al., 1985)
		876	877	877	opx-cpx (Finnerty and Boyd, 1987)
		864	866	869	opx-cpx (Yamada and Takahashi, 1984)
		867	869	872	opx-cpx (Brey and Kohler, 1990)
G107A(i)	ol-opx-cpx-hn-pl-ilm	777	786	795	hn-pl (Holland and Blundy, 1994)
			~ 900		hn-opx (Perchuk et al., 1985)
		922	923	924	opx-cpx (Finnerty and Boyd, 1987)
		910	913	915	opx-cpx (Yamada and Takahashi, 1984)
		896	898	900	opx-cpx (Brey and Kohler, 1990)
G107B	opx-cpx-hn-pl-ilm	784	791	798	hn-pl (Holland and Blundy, 1994)
			~ 790		hn-opx (Perchuk et al., 1985)
		814	815	815	opx-cpx (Finnerty and Boyd, 1987)
		802	805	807	opx-cpx (Yamada and Takahashi, 1984)
		807	809	812	opx-cpx (Brey and Kohler, 1990)
G688	opx-cpx-hn-pl-ilm	828	835	843	hn-pl (Holland and Blundy, 1994)
			~ 785		hn-opx (Perchuk et al., 1985)
		879	880	881	opx-cpx (Finnerty and Boyd, 1987)
		867	869	872	opx-cpx (Yamada and Takahashi, 1984)
G96B	opx-cpx-hn-pl	842	844	846	opx-cpx (Brey and Kohler, 1990)
		822	830	838	hn-pl (Holland and Blundy, 1994)
			~ 800		hn-opx (Perchuk et al., 1985)
		853	853	854	opx-cpx (Finnerty and Boyd, 1987)
	841	843	846	opx-cpx (Yamada and Takahashi, 1984)	
	844	846	848	opx-cpx (Brey and Kohler, 1990)	
Ultra-mylonite zone in massive gabbro (GIII)					
G1004A	cpx-hn-pl-ilm	756	762	769	hn-pl (Holland and Blundy, 1994)

^a Average mineral analyses used, sourced from Christodoulou (1984).

References

- Anderson, H.J., 1989. The 1989 Macquarie Ridge earthquake and its contribution to the regional seismic moment budget. *Geophysical Research Letters* 17, 1013–1016.
- Angelier, J., Mechler, P., 1977. Sur une méthode graphique de recherche des contraintes principales également utilisable en tectonique et en séismologie: la méthode des dièdres droits. *Bulletin Geology Society France* 19, 1309–1318.
- Ballhaus, C., Berry, R.F., Green, D.H., 1991. High pressure experimental calibration of the olivine–orthopyroxene–spinel oxygen geobarometer: implications for the oxidation state of the upper mantle. *Contributions to Mineralogy and Petrology* 107, 27–40.
- Banghar, A.R., Sykes, L.R., 1969. Focal mechanisms of earthquakes in the Indian Ocean and adjacent regions. *Journal of Geophysical Research* 74, 632–649.
- Begin, N.J., 1992. Contrasting mineral isograd sequences in metabasites of the Cape Smith Belt, northern Quebec, Canada: three new bathograds for mafic rocks. *Journal of Metamorphic Geology* 10, 685–704.
- Berthé, D., Choukroune, P., Jegouzo, P., 1979. Orthogneiss, mylonite and noncoaxial deformation of granites: the example of the South Armorican Shear Zone. *Journal of Structural Geology* 1, 31–42.
- Bevins, R.E., Merriman, R.J., 1988. Compositional controls on coexisting prehnite–actinolite and prehnite–pumpellyite facies assemblages in the Tal y Fan metabasite intrusion, North Wales: implications for Caledonian metamorphic field gradients. *Journal of Metamorphic Geology* 6, 17–39.
- Bock, G., 1981. Focal mechanism of an earthquake from the Southern Ocean. *Tectonophysics* 79, T37–T41.
- Boudier, F., Le Sueur, E., Nicolas, A., 1989. Structure of an atypical ophiolite: the Trinity complex, eastern Klamath Mountains, California. *Geological Society of America Bulletin* 101, 820–833.
- Brey, G.P., Kohler, T., 1990. Geothermobarometry in four-phase lherzolites II. New thermobarometers, and practical assessment of existing thermobarometers. *Journal of Petrology* 31, 1353–1378.
- Burg, J.P., Laurent, Ph., 1978. Strain analysis of a shear zone in a granodiorite. *Tectonophysics* 47, 15–42.
- Cannat, M., Bideau, D., Bougault, H., 1992. Serpentinized peridotites and gabbros in the Mid-Atlantic Ridge axial valley at 15°37'N and 16°52'N. *Earth and Planetary Science Letters* 109, 87–106.
- Cannat, M., Mevel, C., Maia, M., Deplus, C., Durand, C., Gente, P., Agrinier, P., Belarouchi, A., Dubuisson, G., Humler, E., Reynolds, R., 1995. Thin crust, ultramafic exposures, and rugged faulting patterns at the Mid-Atlantic Ridge (22–24°N). *Geology* 23, 49–52.
- Carbotte, S.M., Macdonald, K.C., 1990. Causes of variation in fault-facing direction on the ocean floor. *Geology* 18, 749–752.
- Christodoulou, C. (1984) The geology and geochemistry of Macquarie Island. Unpublished Ph.D. thesis, University of Adelaide, Australia.

- Christodoulou, C., Griffin, B.J., Foden, J. (1984) The Geology of Macquarie Island. *ANARE Research Notes* 21. Antarctic Division, Tasmania, Australia.
- Cleary, J., 1966. Amplitudes from Longshot at Australian Stations. *Nature* 211, 954.
- Coffin, M.F., Karner, G.D., Falvey, D.A., 1994. Research cruise yields new details of Macquarie Ridge Complex. *EOS Transactions, American Geophysical Union* 75, 561–564.
- Collot, J.-Y., Lamarche, G., Wood, R.A., Delteil, J., Sosson, M., Lebrun, J.-F., Coffin, M.F., 1995. Morphostructure of an incipient subduction zone along a transform plate boundary: Puysegur Ridge and Trench. *Geology* 23 (6), 519–522.
- Crawford, T., Coffin, M., 1993. Marine geophysical and geological investigations of Macquarie Ridge, Macquarie Island and the Macquarie triple Junction. *InterRidge News* 2, 5–8.
- DeMets, C., Gordon, R.G., Argus, D.F., 1988. Intraplate deformation and closure of the Australia–Antarctica–Africa Plate Circuit. *Journal of Geophysical Research* 93, 11871–11877.
- Denham, D., 1973. Seismicity, focal mechanisms and the boundaries of the Indian–Australian Plate. In: Coleman, P.J. (Ed.). *The Western Pacific: Island Arcs, Marginal Seas, Geochemistry*. University of Western Australia Press, Perth, pp. 35–53.
- Digel, S., Ghent, E.D., 1994. Fluid–mineral equilibria in prehnite–pumpellyite to greenschist facies metabasites near Flin–Flon, Manitoba, Canada: implications for petrogenetic grids. *Journal of Metamorphic Geology* 12, 467–477.
- Duncan, R.A., Varne, R., 1988. The age and distribution of the igneous rocks of Macquarie Island. *Papers and Proceedings of the Royal Society of Tasmania* 122, 45–50.
- Finnerty, A.A., Boyd, F.R., 1987. Thermobarometry for garnet peridotites: basis for the determination of thermal and compositional structure of the upper mantle. In: Nixon, P.H. (Ed.). *Mantle Xenoliths*. John Wiley and Sons, London, pp. 381–402.
- Flinn, D., 1962. On folding during three dimensional progressive deformation. *Geological Society of London Quarterly Journal* 118, 385–433.
- Frohlich, C., Coffin, M.F., Massell, C., Mann, P., Schuur, C.L., Davis, S.D., Jones, T., Karner, G., 1996. Constraints on Macquarie Ridge tectonics provided by Harvard focal mechanisms and teleseismic earthquake locations. *Journal of Geophysical Research* 102 (B3), 5029–5041.
- Girardeau, J., Nicolas, A., 1981. The structures of two ophiolite massifs, Bay-of-Islands, Newfoundland: a model for the oceanic crust and upper mantle. *Tectonophysics* 77, 1–34.
- Goscombe, B.D., Findlay, R.H., McClenaghan, M.P., Everard, J.L., 1994. Multi-scale kinking in northeast Tasmania: crustal shortening at shallow crustal levels. *Journal of Structural Geology* 16, 1077–1092.
- Goscombe, B.D., Everard, J.L., 1997. The Geology of Macquarie Island. Part 1: Igneous field relationships and reconstruction of the Macquarie Island oceanic crust. *Mineral Resources Tasmania Report*. Mineral Resources, Tasmania.
- Goscombe, B.D., Everard, J.L., 1998. 1:10000 Geological Map of Macquarie Island. *Mineral Resources, Tasmania Series of 7 maps*.
- Goscombe, B.D., Everard, J.L., 1999. *EOS Transactions* 80 (5), 50 and p. 55.
- Griffin, B.J., Varne, R., 1980. The Macquarie Island ophiolite complex: mid-tertiary oceanic lithosphere from a major ocean basin. *Chemical Geology* 30, 285–308.
- Griffin, B.J. (1982) Igneous and metamorphic petrology of lavas and dykes of the Macquarie Island ophiolite complex. Unpublished PhD thesis, University of Tasmania, Hobart.
- Harker, R.I., 1964. Dehydration series in the system $\text{CaSiO}_3\text{--SiO}_2\text{--H}_2\text{O}$. *Journal of the American Ceramic Society* 47, 521–529.
- Hayes, D.E., Talwani, M., Christoffel, J.D.A., 1972. Macquarie Ridge Complex. In: Adie, R.J. (Ed.). *Antarctic Geology and Geophysics*. Number 1. International Union of Geological Sciences Series B International Union of Geological Sciences, London, pp. 767–771.
- Hemley, J.J., Montoya, J.W., Christ, C.L., Hosteler, P.B., 1977. Mineral equilibria in the $\text{MgO--SiO}_2\text{--H}_2\text{O}$ system: I. Talc–chrysotile–forsterite–brucite stability relations. *American Journal of Science* 277, 322–351.
- Hoek, J.D., Seitz, H.-M., 1995. Continental mafic dyke swarms as tectonic indicators: an example from the Vestfold Hills, East Antarctica. *Precambrian Research* 75, 121–139.
- Holland, T., Blundy, J., 1994. Non-ideal interactions in calcic amphiboles and their bearing on amphibole–plagioclase thermometry. *Contributions to Mineralogy and Petrology* 116, 433–447.
- Johnson, T., Molnar, P., 1972. Focal mechanisms and plate tectonics of the southwest Pacific. *Journal of Geophysical Research* 77, 5000–5021.
- Jones, T.D., McCue, K.F., 1988. The seismicity and tectonics of the Macquarie Ridge. *Papers and Proceedings of the Royal Society of Tasmania* 122, 51–57.
- Kawasaki, T., Ito, E., 1994. An experimental determination of the exchange reaction of Fe^{2+} and Mg^{2+} between olivine and Ca-rich clinopyroxene. *American Mineralogist* 79, 461–477.
- Lamarche, G., Collot, J.-Y., Wood, R.A., Sosson, M., Sutherland, R., Delteil, J., 1997. The Oligocene–Miocene Pacific–Australian plate boundary, south of New Zealand: evolution from oceanic spreading to strike–slip faulting. *Earth and Planetary Science Letters* 148, 129–139.
- Larson, K.M., Fraymueller, J., 1995. Relative motions of the Australian, Pacific and Antarctic plates estimated by the Global Positioning System. *Geophysical Research Letters* 22, 37–40.
- Ledingham, R.B., 1978. A Macquarie earthquake. *Aurora: ANARE Club Journal Spring*, 135–136.
- Liou, J.G., 1973. Synthesis and stability relations of epidote, $\text{Ca}_2\text{Al}_2\text{Fe--Si}_3\text{O}_{12}(\text{OH})$. *Journal of Petrology* 14, 381–413.
- Liou, J.G., Kuniyoshi, S., Ito, K., 1974. Experimental studies of the phase relations between greenschist and amphibolite in a basaltic system. *American Journal of Science* 274, 613–632.
- Lippard, S.J., Shelton, A.W., Gass, I.G., 1986. The ophiolite of northern Oman. *Memoir of the Geological Society of London* 11.
- Lister, G.S., Snoke, A.W., 1984. *S–C* mylonites. *Journal of Structural Geology* 6, 617–638.
- Mawson, D., 1943. *Macquarie Island: Its Geography and Geology*. Government Printing Office, Sydney.
- Minster, J.B., Jordan, T.H., 1978. Present day plate motions. *Journal of Geophysical Research* 10, 5331–5334.
- Molnar, P., Atwater, T., Mammerick, J., Smith, S.M., 1975. Magnetic anomalies, bathymetry and the tectonic evolution of the South Pacific since the Late Cretaceous. *Geophysical Journal of the Royal Astronomical Society* 40, 383–420.
- Moody, J.B., 1976. Serpentinisation: a review. *Lithos* 9, 125–138.
- Nicolas, A., 1989. *Structures of Ophiolites and Dynamics of Oceanic Lithosphere*. Kluwer Academic, Norwell, MA.
- Nicolas, A., Boudier, F., Ildefonse, B., 1994. Dyke patterns in diapirs beneath oceanic ridges: the Oman ophiolite. In: Ryan, M.P. (Ed.). *Magmatic Systems*. Academic Press, New York, pp. 77–95.
- Nicolas, A., Boudier, F., 1995. Mapping oceanic ridge segments in Oman ophiolite. *Journal of Geophysical Research* 100, 6179–6197.
- Nitsch, K.H., 1971. Stabilitätsbeziehungen von prehnit und pumpellyit-haltigen paragenesen. *Contributions to Mineralogy and Petrology* 30, 240–260.
- Owen, H.G., 1983. *Atlas of Continental Displacement*. Cambridge University Press, Cambridge.
- Passchier, C.W., Simpson, C., 1986. Porphyroclast systems as kinematic indicators. *Journal of Structural Geology* 8, 831–843.
- Perchuk, L.L., Aranovich, L.Ya., Podlesskii, K.K., Lavrent'eva, I.V., Gerasimov, V.Yu., Fed'kin, V.V., Kitsul, V.I., Karsakov, L.P., Berdnikov, N.V., 1985. Precambrian granulites of the Aldan Shield, eastern Siberia, USSR. *Journal of Metamorphic Geology* 3, 265–310.
- Pieters, P.E. and Wyborn, D. (1977) Geological work in Antarctica—1974/75. *Bureau of Mineral Resources, Geology and Geophysics Report* 16, Canberra, Australia.
- Podvin, P., 1988. Ni–Mg partitioning between synthetic olivines and orthopyroxenes: application to geothermometry. *American Mineralogist* 73, 274–280.

- Powell, M., Powell, R., 1974. An olivine–clinopyroxene geothermometer. *Contributions to Mineralogy and Petrology* 48, 249–263.
- Ramsay, J.G., 1979. Shear zones. Proceedings of Conference 8; Analysis of Actual Fault Zones in Bedrock. U.S. Geological Survey Open-file Report 79-1239. U.S. Geological Survey, Washington, DC, pp. 2–35.
- Ramsay, J.G., Graham, R.H., 1970. Strain variation in shear belts. *Canadian Journal of Earth Science* 7, 786–813.
- Romanowicz, B.M.C., Ekstrom, G., 1989. Macquarie Earthquake of May 23, 1989. *EOS Transactions* 70, 699–700.
- Rong-long, C., Ross, C., Ernst, W.G., 1986. Experimental studies to 10 kb of the bulk composition tremolite₅₀–tschermakite₅₀ + excess H₂O. *Contributions to Mineralogy and Petrology* 93, 160–167.
- Rosencrantz, E., 1982. Formation of uppermost oceanic crust. *Tectonics* 1, 471–494.
- Ruff, L.J., Given, J.W., Sanders, C.O., Sperber, C.M., 1989. Large earthquakes in the Macquarie Ridge Complex: transitional tectonics and subduction initiation. *Pure and Applied Geophysics* 128, 72–129.
- Salisbury, M.H., Christensen, N.I., 1985. Olivine fabrics in the Bay of Islands ophiolite: implications for oceanic mantle structure and anisotropy. *Canadian Journal of Earth Science* 22, 1757–1766.
- Sanderson, D.J., Marchini, W.R.D., 1984. Transpression. *Journal of Structural Geology* 6, 449–458.
- Schiffman, P., Liou, J.G., 1980. Synthesis and stability relations of Mg–Al pumpellyite, Ca₄Al₅MgSiO₂₁(OH)₇. *Journal of Petrology* 21, 441.
- Schuur, C.L., Coffin, M.F., Frolich, C., Massell, C.G., Karner, G.D., Ramsay, D., Caress, D.W., 1998. Sedimentary regimes at the Macquarie Ridge Complex; interaction of Southern Ocean circulation and plate boundary bathymetry. *Paleoceanography* 13, 646–670.
- Searle, R.C., 1992. The volcano–tectonic setting of oceanic lithosphere generation. In: Parson, L.M., Murton, B.J., Browning, P. (Eds.). *Ophiolites and their Modern Oceanic Analogues*. Geological Society Special Publication, 60. Geological Society, London, pp. 65–79.
- Selkirk, P.M., McBride, T.P., Keenan, H.M., Adamson, D.A., 1988. Palaeolake deposits and cliff retreat on subantarctic Macquarie Island. In: Gillieson, D., Fitzsimons, S. (Eds.). *Quaternary Research in Australian Antarctica; Future Directions*. Special Publication, 3. Department of Geography and Oceanography, University of New South Wales, Canberra, pp. 45–53.
- Sorlein, C. (1989) Computer program EQUAL AREA JAN89. University of California, Santa Barbara.
- Spear, F.S., 1981. An experimental study of hornblende stability and compositional variability in amphibolite. *American Journal of Science* 281, 697–734.
- Spear, F.S., 1993. Metamorphic phase equilibria and pressure–temperature–time paths. *Mineralogical Society of America Monograph* 1.
- Sutherland, R., 1995. The Australia–Pacific boundary and Cenozoic plate motions in the SW Pacific: some constraints from GEOSAT data. *Tectonics* 14 (4), 819–831.
- Sykes, L.R., 1967. Mechanism of earthquakes and nature of faulting on the Mid-Oceanic Ridges. *Journal of Geophysical Research* 72, 2131–2153.
- Varne, R., Gee, R.D., Quilty, P.G.J., 1969. Macquarie Island and the cause of oceanic linear magnetic anomalies. *Science* 166, 230–232.
- Varne, R., Rubenach, M.J., 1972. In: Hayes, D.E. (Ed.). *Antarctic Geology II. The Australian–New Zealand Sector*. Antarctic Research Series, 19. Australian Geological Society, Canberra, pp. 251–266.
- Veevers, J.J., 1990. Antarctica–Australia fit resolved by satellite mapping of oceanic fracture zones. *Australian Journal of Earth Sciences* 37, 123–126.
- van der Wal, D., Vissers, R.L.M., Drury, M.R., Hoogerduijn Strating, E.H., 1992. Oblique fabrics in porphyroclastic Alpine-type peridotites: a shear-sense indicator for upper mantle flow. *Journal of Structural Geology* 14, 839–846.
- Walcott, R.I., 1978. Present tectonics and Late Cenozoic evolution of New Zealand. *Geophysical Journal of the Royal Astronomical Society* 52, 137–164.
- Weissel, J.K., Hayes, D.E., Herron, E.M., 1977. Plate tectonic synthesis: the displacements between Australia, New Zealand, and Antarctica since the late Cretaceous. *Marine Geology* 25, 231–277.
- Wicks, F.J., O’Hanley, D.S., 1988. Serpentine minerals: structures and petrology. In: Ribbe, P.H. (Ed.). *Hydrous Phyllosilicates*. Reviews in Mineralogy, 19. Mineralogical Society of America, Washington, DC, pp. 303–312.
- Williamson, P., Johnson, B.D., 1974. Crustal structure of the central region of the Macquarie Ridge Complex from gravity studies. *Marine Geophysical Researches* 2, 127–132.
- Williamson, P., 1988. Origin, structure and tectonic history of the Macquarie Island region. *Papers of the Proceedings of the Royal Society of Tasmania* 122, 27–43.
- Witt-Eickschen, G., Seck, H.A., 1991. Solubility of Ca and Al in orthopyroxene from spinel peridotite: an improved version of an empirical geothermometer. *Contributions to Mineralogy and Petrology* 106, 431–439.
- Wood, R., Lamarche, G., Herzer, R., Delteil, J., Davy, B., 1996. Paleogene seafloor spreading in the southeast Tasman Sea. *Tectonics* 15, 966–975.
- Yamada, H., Takahashi, E., 1984. Subsolidus phase relations between coexisting garnet and two pyroxenes at 50–100 kbar in the system CaO–MgO–Al₂O₃–SiO₂. In: Kornprobst, J. (Ed.). *Kimberlites II, the Mantle and Crust–Mantle Relationships*. Elsevier Science, Amsterdam, pp. 247–255.